ISSN 0097-8078, Water Resources, 2023, Vol. 50, No. 5, pp. 709–731. © Pleiades Publishing, Ltd., 2023.
Russian Text © The Author(s), 2023, published in Vodnye Resursy, 2023, Vol. 50, No. 5, pp. 561–584.

STUDIES OF THE PROCESSES OF INTERACTION BETWEEN LAND AND THE ATMOSPHERE AND THE HYDROLOGICAL EFFECTS OF CLIMATE CHANGE

Utilization of Remote Sensing Data in the Simulation of the Water and Heat Regime of Land Areas: A Review of Publications

E. L. Muzylev*

Water Problems Institute, Russian Academy of Sciences, Moscow, 119333 Russia

**e-mail: muzylev@iwp.ru*

Received January 31, 2023; revised January 31, 2023; accepted March 20, 2023

Abstract—The article presents a revue of the estimates of soil surface moisture, soil water content, and evapotranspiration as elements of water and heat regimes of land surface areas at various spatial scales, made with the use of remote sensing data for Earth in various spectral ranges. In most cases considered in the study, such estimates were obtained with the use of land surface models. A special section is focused on the results of estimating soil surface moisture and water content using satellite data from microwave range, including radar data. Estimates of soil surface moisture content obtained with the use of neural networks are presented. A brief description is given to international hydrological–atmosphere experiments carried out under world research projects aimed to obtain data on the processes of moisture and heat exchange between the land surface and the surface atmosphere layer. Land surface, satellite, and model databases that have been formed using the results of studies in the field under consideration since the mid-1980s are reviewed. Prospects of further studies based on the development of new multispectral instrumentation, the creation of new databases, and the use of a new generation of satellites—global-coverage microsatellites with high-resolution sensors are presented.

Keywords: satellite data, simulation of water and heat exchange processes, water and heat regimes, land surface characteristics, soil water content, evapotranspiration, spatial resolution

DOI: 10.1134/S0097807823700021

INTRODUCTION. THE PROBLEMS UNDER CONSIDERATION

The interest to the use of remote sensing data in the simulation of water and heat regimes in land areas has formed by the mid-1980s, when, on the one hand, rapid development of land surface models began [7, 39, 71, 132], and, on the other hand, the progress in the development of new optoelectronic and radio instrumentation installed on space vehicles, along with remote measurements of land surface characteristics provided data on the space and time variations in those characteristics [68, 126–128, 134], which could be used to extend the information base of the models [13, 110, 133, 142]. Combining these two approaches into one general direction of research on the processes of moisture and heat transfer prompted the conduct of hydrological–atmospheric field experiments HAPEX-MOBILHY (1986) [14, 124], HAPEX-SAHEL (1992, 1991–1993) [51], FIFE (1987, 1989) [129, 130], KUREKS (1988, 1991) [70, 72], EFEDA (1991–1994) [26, 27], BOREAS (1993–1996) [108, 131], MOPEX (1996–2003, 2004–2009) [15, 42, 123], etc., the organization, under the World Climate Research Program WCRP (since 1980), of a project of global energy and water exchange GEWEX (since 1990) [141], as well as the implementation under international geospheric–biospheric program IGBP (1987–2015) [62], of the main BAHS program (since 1993) [24, 59]. The objective of practically all field experiments mentioned above was to measure the land surface (LS) parameters, including the characteristics of vegetation, as well as water and heat fluxes and the fluxes of matter (as a rule, with the incorporation of the data of earth remote sensing (ERS)), with the aim to evaluate the model parameters of the interaction between LS and the atmosphere and to reveal the role of the biosphere in this interaction. The objective of the GEWEX project is to study the energy and water cycles of the Earth and to evaluate the water and energy fluxes at the regional and global scales [141]. The objective of the IGBP program is the formation of the knowledge on the behavior of various elements of the Earth system under the effect of physical, chemical, and biological processes, as well as the description of the anthropogenic effect on global processes involved in the water cycle as well as the cycles of carbon, nitrogen, sulfur, and phosphorus. The BAHC project was intended to study the effect of biosphere elements, in particular, vegetation, on the dynamics of the hydrological cycle by carrying out experiments and simulating processes of the formation of energy, water, carbon dioxide fluxes, and sediments in the system

soil–vegetation–atmosphere for various space and time scales. As the considerable effect of vegetation on the formation of these fluxes makes it an important factor of hydrological cycle regulation and climate formation, an important task of the project was the identification of vegetation cover transformations caused by human activity and considered as a factor of climate changes. The BAHC program also included studying the effect of the climate and human activity on the accumulation and river transport of sediments [59].

The data collected by surface measurements and ERS, as well as by simulating moisture and heat exchange were, to a certain extent, combined to form regional and global databases on LS and weather characteristics, including those extending up to now and newly formed. These include the systems and databases GCOS [50], NCEI NOAA [102]—ISD [63], and LCD [77]. The observation system GCOS, created in 1992 with the support of WCRP, determined 50 key climate variables applicable to global climate observations. Considerable contribution to GCOS was made by the World Integrated Global Observing System WIGOS WMO and the World Hydrological Cycle Observing System WHYCOS with databases. ISD is a global database of hourly and synoptic observations of the characteristics of LS and surface atmosphere layer from numerous (more than 100) sources from more than 20000 stations. These data are collected in a common format and combined to form a single data model. The LCD base contains sets of climate data, obtained by generalization of local climate conditions for more than 2500 weather stations and airports of the USA. ECOCLIMAP-I database [5, 91] and ECOCLIMAP-II [46], improved with the use of datasets for European territory, are used to initialize (to specify the initial conditions and parameter values) models of SVAT type for meteorological and climate models (at all horizontal scales). At the formation of ECOCLIMAP-I database for regions with homogeneous vegetation, identified by combining LS maps and climatic maps with the incorporation of AVHRR data with the use of fields of *LAI* values, constructed by these data, the values of all model parameters were constructed (the characteristics of vegetation cover and weather characteristics) [91]. The construction of ECOCLIMAP II database used a more complex specification of the examined areas by LS and plant types (some clusters) and incorporated two proxy variables *NDVI* and *LAI*, determined by data of radiometers SPOT/Vegetation and MODIS, respectively. The values of all parameters of model ISBA, class SVAT (developed by Météo France) were obtained for these clusters [46]. The global database ISLSCP II, formed in ORNL DAAC NASA under the project with the same name, a part of GEWEX project, contains archived overall databases of 1986–1995 on the LS characteristics; hydrological, meteorological, radiation, and soil characteristics with resolution of 1/4°, 1/2°, and 1° [29]. These archives were supplemented by sets of estimates of LS–NDVI, albedo, LAI, and other characteristics by satellite data of sensors AVHRR, MODIS, SPOT/Vegetation, and VIIRS over later years [29]. The part "Hydrology and Soils" in this database contains, for example, sets of estimates of the proportion of soil moisture available for plants, estimates of the monthly runoff volumes, datasets on daily, pentad, and monthly total precipitation, as well as data on precipitation, required for solving climate problems [64], as well as many other datasets.

In the recent 25 years, global and continental GIS-databases in different fields were developed including hydrological, climate, and soil ones. The global databases include, for example, USGS database LCI on land cover; IRI/LDEO CDL database of the Earth Institute, the University of Columbia and the Observatory of Land Lamont-Doherty at the same university, containing datasets from more than 300 climate models and databases; the database of soil characteristics HWSD FAO [45], containing data on the texture parameters, depths, and soil acidity; the global elevation database ASTER GDEM with a 30-m resolution, constructed based on satellite images of ASTER radiometer; a set of renewable maps of soil properties and classes in the world with a resolution of 1 km (SoilGrids1km—soil property and class maps), compiled with the use of modern statistical methods; the global database CHELSA with a resolution of 1 km, the first implementation of which [66] contained sets of air temperature estimates, formed at a statistical decrease of the scale, and monthly precipitation totals, obtained by data of climatic reanalysis ERA-Interim with the use of wind speed, valley slope aspects, and the heights of the atmospheric boundary layer. The second implementation [30] included sets of monthly estimates of air pressure deficit, incoming short-wave radiation, potential evapotranspiration, climatic water humidity index, and area water index over 1980–2018. These estimates were formed based on the results of calculation with combined data obtained by joining the data derived by a decrease by delta-method of the scale of time series of relative air humidity near land surface and the proportion of cloud area along with a mechanical decrease of the scale for the data on temperature, precipitation, and solar radiation. The GIS-databases of global level also include OpenAerialMap with an open license, which provides a set of instruments for the search, exchange, and use of images from satellites and UAV (Unmanned Aerial Vehicle) and OpenLandMap, containing sets of various data on the Earth (the so-called Earth mask) on LS, vegetation, soils, climate, information on terrain etc.

One of the continental GIS bases is the European base ESDAC [112], containing information of the European Soil Data Base, sets of estimates of soil erosion, the amount of organic carbon in soil, its biodiversity, as well as data of LUCAS (results of laboratory physical and chemical analyses of the top (0–20 cm) soil layer for samples taken at more than 20000 sites in

the European Union countries), etc. We will also mention two GIS-databases for USA: NGDC—a base of digital elevation models (DEV) in free access, data on LS, seismological and other data, as well as a soil database of US Ministry of Agriculture (USDA NRCS). The latter can be combined with various datasets with the use of an online mapping instrument Web Soil Survey.

In the recent decades, considerable attention was also paid to the formation of ERS databases on LS and weather characteristics for their use in simulating the processes of moisture and heat exchange. For example, the sources of such data in open access include: the database USGS Earth Explorer for various territories, containing Landsat data, unclassified 1960–1970 data from satellites of CORONA system, geospectral data, obtained with the use of NASA Hyperion spectrometer; Sentinel Open Access Hub with survey data of twelve-channel multispectral camera in the ranges from the visible to SWIR from Sentinel-2 board at 10-m resolution in VNIR ranges and the survey data with the use of SAR in the microwave C-range from the board of Sentinel-1 with a resolution from 5 × 5 to 20 × 40 m at the quality of images poorer than that of Sentinel-2; NASA Earthdata Search base (the majority of data enters into it from the NASA DAAC center), representing products for the analysis of Earth processes, is a high-class source of data on the global land use and vegetation cover and contains specialized satellite data, such as the types of permafrost and water–swamp fields; the set of NOAA Data Access Viewer, containing satellite images, aerial photographs, and images obtained with the use of lidars; database of DigitalGlobe—a commercial operator of high-resolution satellites GeoEye-1, QuickBird, IKONOS, WorldView group, from which the entire library of 30-cm images DigitalGlobe can be loaded free of charge. In the case of any natural disaster, the Open Data Programme DigitalGlobe for help presents, free of charge, satellite images of fires, floods, hurricanes, typhoons, and earthquakes. Also, data samples can be obtained free of charge, including contours of buildings, elevations, stereo images, and images in real color. The database of the Geo-Airbus Defense company, a commercial supplier of satellite images from SPOT, Pleiades, and RapidEye satellites, includes a set of image samples; however, the choice of satellite images free of charge is very limited. The proposed samples include optical images SPOT with a resolution of ≤1.5 m, radar images TerraSAR-X with a resolution of ≤3 m and horizontal sections of DEM WorldDEM with a resolution of 12 m (more accurate than DEMs ASTER, and SRTM). The database of the National Institute of Space Studies of Brasilia (INPE) is a catalogue of INPE images, similar to the library for free of charge loading of satellite images. The major portion of this catalogue consists of images from CBERS Chinese–Brazilian satellites, and all the data refer to the South America and Africa. It will also contain the data from CBERS-4 [114], Indian satellite ResourceSat and British UK-DMC 2. The global DEM AW3D30 with a 30-m resolution is an open-access set of world level data based on the results of surveying from onboard satellite ALOS JAXA by PRISM instruments in the optical range with a resolution of 2.5 m. This set was formed based on a dataset from DEM version with a 5-m grid World 3D Topographic Data, which now contains the most accurate data on elevations at a global scale. The web-site VITO Vision presents free of charge images of satellites PROBA-V (PROBA-Vegetation), SPOT-Vegetation, and MetOp. These satellites with a low-resolution cut patterns of vegetation on the Earth surface. The Satellite Land Cover database at a global level gives the sources of data from Landsat, MODIS, and AVHRR on the land cover, which allow observing quantitative changes in its characteristics all over the world—for territories with various geological and hydrological conditions, various vegetation and agricultural features, as well as for urban areas. An extending database, used in the simulation of moisture and heat exchange, is the GLASS base, the number of satellite products in which increased from 5 in 2012 [84] to 14 in 2020 [83]. Now, the database contains datasets on *LAI*, broad-band albedo *A* and longwave radiation capacity *E*, incoming shortwave *R* and resultant longwave radiation, photosynthetic active radiation *PAR* and its adsorbed fraction *FAPAR*, LS temperature *LST*, projective cover by vegetation *B*, evapotranspiration *ET*, latent heat flux *LE*, etc. [83]. The duration of uninterrupted measurements of *LAI*, *A*, *E*, *R*, and *PAR* exceeds 35 years (since 1981 until now) without gaps, the space and time resolution of the former three is 1–5 km and 3 h, respectively. The Landsat USGS database [74], which has been updated with the results of sounding from Landsat-9 since February 2022, is also widely used [75]. The global data of Landsat-9 OLI-2 in nine ranges (VNIR, SWIR, and others) with a resolution of 30 m and TIRS-2 in two thermal ranges [76] enable numerous estimates of the characteristics of PP and atmospheric boundary layer, as required for the implementation of hydrological models. The use of data on land classification, carried out in accordance with IGBP classification scheme, from the dataset of terrestrial ecosystem classification MODIS MOD12Q1 [98], as well as daily, eight-day, and monthly data on the albedo and NDVI, obtained by MODIS measurements with a resolution of 1 angular minute [97], combined with Landsat-9 data, will improve the accuracy of calculations using these models.

The launch in the recent 15–20 years of the satellites mentioned above with instruments of either high or low resolution has resulted in the appearance of additional data that can be used in models for areas of various scales, from local to global, and, therefore, the formation of appropriate databases. These are GLCC [87], GLDAS [120], NLDAS-1 [96], and NLDAS-2

[155] and other LDAS [154]. The launch into orbit of satellites MetOp-A, -B, -C, SMOS, SMAP, GCOM-W1, and GCOM-C1, as well as above-mentioned Sentinel-1, and others with active or passive microwave range sensors, as well as with radars, allowed the obtained data to be used to calculate soil moisture content in areas with a size determined by satellite equipment resolution and varying from an individual field to a continent [44, 69, 107, 116, 118, 137, 138, 145]. The satellite imagery with the use of synthetic aperture radars, which has been actively developing in recent years, attracts the interest of users because of its all-weather capability, i.e., the independence of cloudiness, which is typical of data of VNIR ranges, and the ability of radio waves emitted from a satellite to penetrate under tree crowns and next to be recorded in the form of a reflected signal, thus presenting data without time delays. Examples of the implementation of this technology include 1-st generation satellites (2007–2012) TerraSAR-X, Radarsat-2, COSMO-SkyMed, TanDEM-X and 2-nd generation (since 2018): SGS-1, PAZ. Note also that the Sentinel-1 images with 10-m resolution with resurvey within 6–12 days were found to be acceptable for the established community of SAR data users. Now these data are used to study Antarctic icebergs and to reveal environmental changes, as well as to map the effects of natural or anthropogenic impacts. Examples of such use are tracing the effect of explosions, destruction, forest fires, and flood scales; monitoring marine and coastal zones, including oil spills at tanker accidents; monitoring of land, in particular, determining the location of land subsidence and domains subject to the risk of collapses and landslides; studying the state of vegetation (the formation of canopy, the density and growth rates of crops) and the specific features of agricultural activities (the determination of field boundaries and sizes, as well as the time of planting and harvesting). At the passage in the recent 5–7 years to the formation of constellations of small-size microsatellites with a weight of <100 kg, due to the much lower cost of their launch compared with the conventional satellites, the potential of the use of SAR data have increased dramatically. Finnish microsatellite ICEYE-X1 appeared in 2018, followed by 16 other satellites of ICEYE company; satellites SAR Denali (2018) and Sequoia (2020) were launched by Capella Space (USA), followed by 5 global level satellites with hourly time resolution. The maximal number of CubeSat microsatellites (almost 200) was launched by the Planet company. Their data are actively used to solve the problems described above.

In addition to the incorporation of data from various carriers in the simulation—conventional satellites with equipment of various spectral bands, microsatellites with VNIR sensors and radars, aircrafts, and UAV, these data are often combined with models to form appropriate databases, e.g., GLDAS Noah database—a symbiose of the Global Land Data Assimilation System and LSM Noah. Such combination contains a larger volume of data than the results of common observations [92, 143]. The sets of simulation results thus formed are compared with the results of measurements collected in databases created under programs NASA GRACE [173] and its continuation (since 2018) GRACE-FO [52] which are among the most informative. They are supplemented, in addition to the conventional data, by the data of ICESat-2 satellite [36, 60, 61] and will be supplemented by the data from WCOM [135–137] and SWOT [23, 43, 54] scheduled for launch. In the implementation of the programs analogous to GRACE-FO, the appropriate databases of terrestrial and satellite data are also extended, along with the data of reanalysis and the results of simulating the processes of moisture and heat exchange, e.g., OSCAR/Surface and OSCAR/Space [109], working in the WIGOS system [149, 150].

The development perspectives of satellite technologies for evaluating the characteristics of land surface and the surface layer of the atmosphere and the use of the obtained estimates for simulating moisture and heat exchange include the construction of new high-resolution multispectral instrumentation, the formation of vast databases, including cloud, and methods for their processing and assimilating in models. The acquisition of such data with the use of numerous microsatellites with low launch costs and with sensors in various ranges (from VNIR to microwave), showing a high (1.5–4 m) resolution, and covering land surface several times a day, is also highly demanded and promising.

Within the range of problems described above, this review will consider the issues of satellite data utilization in simulating elements of water and thermal regimes of land areas, i.e., the vertical fluxes of moisture and heat, and soil moisture content.

USING REMOTE SENSING DATA IN SIMULATING ELEMENTS OF WATER AND HEAT REGIMES OF LAND AREAS

The Use of Satellite Data in Simulating Vertical Fluxes of Moisture and Heat

Simulating the water and heat regimes of various territories implies reproducing the dynamics of soil water content, evapotranspiration ET (i.e., the total evaporation, including evaporation from bare soil and transpiration by plants), the vertical heat fluxes LE and H, as well as other components of the hydrological cycle, commonly, with the use of models of water and heat exchange between the land surface and the atmosphere, for example, of LSM class, containing equations of water transfer and heat conduction [9, 111, 115, 140]), or balance models of the type of SEBAL, METRIC, SEBS, TSEB, etc. [20, 21, 80, 88]. The information basis of LSM is the sets of soil, vegetation,

and snow cover characteristics, used as input variables [8, 9, 93, 101, 140]. Under conventional approaches, these values were derived from ground observations, while now they are mostly taken from Earth remote sensing. These data are used in LSM to evaluate parameters, e.g., the characteristics of soils and LS; to reveal precipitation zones and amounts; to specify the initial conditions for the model, e.g., soil moisture SM, and to construct time-varying estimates of LS state, e.g., snow water equivalent *SWE*. The set of hydrological characteristics used in LSM and the methods for their assimilation in models are given in [55]. Estimates of some of these characteristics, i.e., vegetation index *NDVI*, LS emissivity *E*, vegetation cover fraction *B*, leaf area index *LAI*, land surface temperature *LST*, and precipitation, were constructed with the use of the developed procedures for thematic processing of measurement data in the visible and IR channels of radiometers AVHRR/NOAA, VIIRS/SNPP, MODIS/Terra, and Aqua, MSU-MR/Meteor-M, SEVIRI/Meteosat [1–4, 10, 11]. In [93], the values of albedo, *NDVI*, and *LAI* were determined using MODIS data. Many studies in this field, carried out with the use of balance models were aimed to obtain estimates only of *ET* or *LE* [12, 22, 32, 144, 147, 160]. In such studies, the values of these variables were determined by different methods: calculated by Penman-Monteith [80, 88, 144] or Priestley–Taylor [32], evaluated with the use of lysimeter measurement data [22, 144], or as a residual term in the radiation balance equation [12, 22, 82, 144, 147], by measurements of flows from towers [80, 88, 153] or scintillometers with a large aperture LAS [80], or estimated based on data of MODIS/TERRA (product MOD16A2) and MODIS/AQUA (MYD16A2) [80, 144]. In [16], the *LE* (and *ET*) and *H* fluxes were calculated using the SEBAL model, in whose equations the albedo and *LST* values were introduced, which were determined using data from the OLI and TIRS sensors of the Landsat-8 and MODIS/Terra satellites (the product MOD09A1). The error in *ET* estimates did not exceed 0.35 mm/day and lied between 11 and 12.5%, and that for *H* estimates lied between 26 and 35%. The study [103] gives estimates of subsoil water level at the construction of its regression dependences on the potential evapotranspiration, calculated with the use of a balance algorithm of SEBAL model. A common feature of all these models is the use of data on vegetation characteristics—*NDVI*, *E*, and *LAI*, obtained from data of MODIS [32, 144, 147], VIIRS [80], Landsat-5, -8 [22, 103, 147], as well as data on heat fluxes, which are used to calculate *LST* and *LE*, determined by data of MODIS and Landsat [32, 144, 147], Landsat-5, -8 [22, 49, 103] with a resolution of 30–120 m, MODIS and VIIRS [80], and ASTER [88]. Measurements of airborne radiometers are also used to obtain estimates of *NDVI*, *B*, and *LAI* [153], as well as heat fluxes [49]. The latter estimates are compared with the results of measurements from "flux towers" [153]. Estimation of the vertical fluxes of moisture and heat at different levels above the land surface were also carried out in the framework of a complex experiment LAFE [152], in which Doppler lidars were used to determine wind speed, air temperature and absolute humidity; airplane and helicopter data on an area 10 × 10 km were used to determine the albedo, *NDVI*, *LAI*, and *LST*; soil moisture was determined by network data; radiation fluxes were measured by vortex covariation method on flux towers installed on SEB-stations. The time resolution of lidar data was 1–10 s, and their space resolution was 30–300 m. In many studies, a part of source data was taken from satellite and surface databases; thus, in study [12], a set of plant characteristics was loaded from archives SPOT-Vegetation data and Global Land Cover Map, and estimates of *LST* and radiation fluxes, from LSA SAF database with a 15-min time resolution and 3-km space resolution.

A similar approach was implemented at a global level in studying the agreement between estimates of evapotranspiration, obtained with the use of satellite data by three different methods and input data sets, including CSIRO-PML [163], MOD16(A2) [99], and GLEAM [86, 89, 90, 94, 95], as well as estimates of precipitation based on GPCP data [57] and changes in soil water content by GRACE data [92] for the basins of Lake Erie, the Aral Sea, and the rivers of Colorado and Niger [86]. The spatial resolution was 0.5° for MOD16 (A2), 0.25° for CSIRO-PML and GLEAM, 1° for precipitation GPCP (1DD v1.2) [58], and 333 km for GRACE. Estimates of vegetation cover characteristics (*NDVI*, *LAI*, etc.), the data on *LST*, radiation fluxes, weather data, including precipitation, were taken from various bases and archives. The increase in the last 3–4 years of the amount of information used to estimate the vertical moisture and heat fluxes increases the possibilities for implementing modern LSM such as SURFEX, JULES, ORCHIDEE, CLM5, and CABLE, for territories at various space scales with the use of mosaic subgrid structure, when using a mosaic subgrid structure, which makes it possible to disaggregate sets of required estimates of water and energy characteristics from satellite and ground-based databases [25, 48].

The Use of ERS Data for Evaluating Soil Moisture Content

The need for estimates of soil water content *W* for territories of different size is determined by the significance of this characteristic as a component of their water balance—an indicator of the state of water resources. For example, K. Zhang et al. [162] evaluated changes in subsurface water content for 168 river catchments as an overall response to global changes in the values of precipitation, evapotranspiration, and runoff volumes. The data on subsurface water content were taken from GRACE information; the estimates

of soil and vegetation water content, water content on land surface, as well as snow water equivalent were compiled from GLDAS databases; two datasets on precipitation were taken from CRU and GPCC databases. Estimates of evapotranspiration were formed using MODIS (MOD16A2) data and taken from GLDAS database, the values of potential evapotranspiration were taken from CPU dataset; and the data on runoff, from study [37]. A digital map for 168 catchments was obtained from GRDC. The contribution of precipitation to the global changes of subsurface water content, determined by GRACE data was 42.6%, that of evapotranspiration was 43.2%, and that of runoff was 14.2%. The obtained results can illustrate the possible structure of such changes under changing climate. The water content W are also an important characteristic of available water supply, they determine the dynamics of plant growth and, as a consequence, agricultural production, which can be seen in the case of deficiency of such reserves and droughts. Estimates of W are also required for calculating runoff characteristics and forecasting floods and freshets, especially, in large rivers.

Soil Surface Moisture Estimates and Water Content of Its Active Layer Using Microwave Remote Sensing Data

In the recent 20 years, the number of estimates of W based on ERS data of the microwave range and obtained at any weather has increased considerably. Depending on the problem to be solved, these estimates were carried out for territories with areas ranging from a few to hundreds of thousands of square kilometers with the use of the measurement results with radiometers AMSR-E/Aqua [111] and AMSR-2/GCOM-W1 [6, 107, 138] in C-, X-, K-, Ka-, and W-ranges with a resolution for AMSR-2 from 35 × 62 km at a frequency of 6.9 HGz to 3 × 5 km at a frequency of 89.0 GHz [6, 107]; radiometer MIRAS of SMOS satellite in L-range with a mean resolution of 43 km [69]; radiometer and radar of SMAP satellite in the same range with a resolution of radiometer of 40 and radar of 3 km [44, 118]; scatterometer ASCAT/MetOp-A, -B, -C in C-range with a resolution of 12.5 km [19, 145]; radar of satellites Sentinel-1A, -1B within the same range with a resolution from 5 × 5 to 25 × 100 m [17, 18]. Since the spatial resolution is proportional to the antenna diameter and inversely proportional to the wavelength, at small wavelengths, an antenna of large diameter is required to obtain high resolution at sounding from a height of several hundred kilometers, which causes considerable engineering problems [69]. Note that, to solve some practical problems under H-SAF [56], a procedure was proposed for disaggregation of the estimates of soil surface humidity (SSH) using ASCAT data with a resolution from 25 to 1 km, based on the use of a linear regression equation with the incorporation of the ASAR radar data from ENVISAT satellite and in-situ data [145]. At the described scatter in the microwave equipment resolution, the values of W can be estimated at a global and regional scale, at a level of individual river catchment, and even a field. L. Brocca et al. [28] used data of an AMSR-E/Aqua radiometer (with the use of three different algorithms) and an ASCAT/MetOp scatterometer to evaluate SSH down to the depth of 5 cm in 17 areas in Italy, Spain, France, and Luxemburg. An exponential filter was used to calculate soil moisture SM in the root zone. The correlation between the obtained estimates and observation data was largest for the results based on ASCAT data for all areas in France and central Italy; the results for other regions are identical. It was also found that an increase in vegetation density leads to a decrease in the reliability of all satellite estimates of SM. The estimates of SM formed for various applications with the use of measurement data from microwave range sensors, such as AMSR-E, TRMM-TMI, SSM/I, WindSat, ERS-1, and -2, ASCAT, as well as SMOS and, later, SMAP, obtained with the use of LSM or reanalysis results, as well as from prognostic centers, e.g. ECMWF or GLDAS and GSWP databases, were combined into ISMN in 2011 [41, 65]. The calibration and verification of the satellite and model estimates of soil moisture were made using in-situ measurement data with a 1-h interval from reliable sources. These data provided information on the space and time variations of SM at different scales. W.A. Dorigo et al. [41] give a review of direct and indirect methods of in-situ SM measurements (gravimetric, with the use of neutron humidimeter and a cosmic ray neutron detector, by the difference between the dielectric constants of soil components and water, with the use of tensiometers, by changes in soil temperature associated with its water content, as well as other methods). As of May 2011, ISMN contained data of 16 regional networks and more than 500 stations in Italy, France, the United States, Russia, Mongolia, Australia, France, West African countries, and others for a period from 1952 to 2011, and this database was expanded in the following years.

J. Shi et al [137] used airborne radiometer measurements of the L- and S-, as well as L- and C-ranges for various space scales to construct SM profiles from 0.1 to 0.4 m in depth, which were compared with measurement results. In this case, the main interfering factors were surface roughness and the presence of vegetation. These results showed that the joint use of L-band and S-band devices improve the accuracy of SM estimation due to the better correction of the effects of vegetation. In addition, the data of observations in the S- and C-bands have a higher spatial resolution than that of data in the L-band; therefore, they can be used to reduce the scale of L-band observation data from, for example, SMOS and SMAP and later WCOM satellites. Since the microwave band data are used to directly estimate the surface (0–3 cm) soil

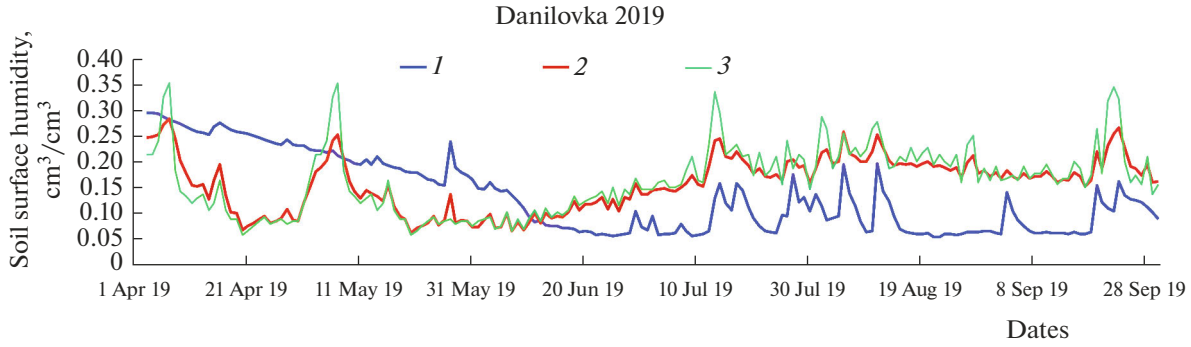

Fig. 1. Soil surface humidity calculated with the use of the model (*1*) by data of ground measurements and (*2*) with the use of evaporation estimates obtained with the use of ASCAT/MetOp data, and (*3*) determined directly by ASCAT measurements. Danilovka Agrometeorologial Station (Volgograd province). 2019 Vegetation season.

layer, the water content of its active layer are evaluated with the use of several approaches. The first approach consists in simulating the process of water transport into deeper soil layers with the use of *SWI* time series, which have an exponential autocorrelation function with a characteristic time that is consistent with the theoretical expectation time and observation results [145]. The second approach is based on the application of extended Kalman filter, which takes into account the errors of the prognostic model without limitations on the time interval of acquisition of earlier satellite data with the division of the soil mass into four layers: 0–7, 7–28, 28–100, and 100–289 cm [33, 34, 73, 120, 145]. The studies [116, 118] use Kalman ensemble filters, in which their ensembles are used to estimate the covariation matrix of forecast errors. The source information used in the studies are ASCAT data in [33, 34, 73, 120, 145], SMAP data in [118], and Sentinel-1 data in [116]. Under the third approach, W is estimated with the use of LSM. In SVAT models, the vertical profiles of soil moisture content are calculated with the use of water transfer and heat equations [8, 9]. The estimates of the characteristics of vegetation, precipitation and *LST* are constructed using measurement data from meteorological satellites. In the calculation of water content, daily SSH composites, formed based on ASCAT/MetOp data, were used at each time step to specify the initial profiles of *SM* as well as to evaluate evaporation from soil surface with the use of bulk-formulas at each time step [8, 101]. Examples given in Fig. 1 show time variations of SSH over the vegetation season, constructed for a station in Volgograd region based on ASCAT data and by simulation results, and Fig. 2 shows the distribution of soil water content in a part of the Central Chernozem Region of Russia (TsChR) for a day in the vegetation season of 2017, calculated by the model with the use of SSH estimates based on ASCAT data and by surface data [101].

LSM Noah [35, 105] is also used to evaluate values of W (at both global and regional scales). In [161], such estimates obtained with the use of this model, associated with GLDAS database, and with the use of ECV, European reanalysis ERA-Interim, and MERRA data with a spatial resolution of 0.25° × 0.25°, 0.5° × 0.5°, and 1° × 1°, were compared with the results of 100 in situ observations for three areas of Himalaya–Tibet plateau. In this case, Noah model generally showed better results. We note the difference between the used data sets. GLDAS-1 and GLDAS-2 are databases of estimates of LS and fluxes, which were formed by joining the results of satellite and ground-based measurements with the use of LSM and data assimilation methods. In ECV, the sets of W estimates are combined from the measurement data of various sensors from radiometer SMMR/Nimbus-7 to scatterometer ASCAT/MetOp. In ERA-Interim, the results of reanalysis were obtained at an alternative regime of data assimilation with the use of 6-hour cycles of analysis, and contain estimates of W for four soil layers (0–7, 7–28, 28–100, and 100–289 cm) [158]. MERRA is a set of reanalysis assimilation results, containing ERS and ground-based observations of the atmospheric characteristics, as well as radiation data from probes, and wind data from scatterometers. LSM Noah GLDAS along with other three models—BHOA [47], ERA-Interim TESSEL, and LISFLOOD [31]—and satellite data ESA CCI was used to evaluate variations of soil surface moisture and water content of its root layer with the aim to compare them with in-situ data from eight sites in Argentinian pampa [139]. It was found that the time distributions of soil water content constructed based on the data of model and satellite estimates are incorrect in some cases, and to extend the possibility for detecting droughts or overmoistening with the use of LSM, it is necessary to have more accurate weather data and the values of soil characteristics.

Miralles et al. [94] calculated the soil water content W in the root zone for global scale with the use of GLEAM model with balance equations solved by difference scheme for successive soil levels. The input variables were the meltwater volume and the total rain

precipitation minus the volume of moisture intercepted by plants, and the output variables were the values of evaporation and moisture infiltration into deeper soil layers. The estimates of water balance were corrected for each day with the use of the Kalman filter for satellite observations. The evaporation was calculated by the Priestley–Taylor formula for bare soil, low (0–5, 5–100 cm), and high (0–5, 5–100 cm and 1.0–2.5 m) vegetation at the use of estimates of SSH, LST, plant cover density, and snow depth, obtained using measurement data from AMSR-E/AQUA radiometer in the 36.5 GHz band with a resolution of 12 km and within the 6.9 GHz with a resolution of 56 km. Precipitation was determined by observations with a half an hour interval within IR-range by geostationary satellites GOES, GMS, and Meteosat for increasing the volume of their more accurate estimates in the microwave range by data of sensors AMSU-B, SSM/I, TMI, and AMSR. The set of data on vegetation *VCF* product was formed using MODIS data (MOD44B package). Air pressure was calculated by the barometric height formula with the use of digital elevation model. Evaporation estimates were verified using data of FLUXNET stations in Europe and USA for the most typical climate conditions and vegetation types. Such approach based on the use of GLEAM to evaluate the water content *W* of the root layer and evaporation *ET*, was also used in [95]. Both values were calculated with the use of water balance equation with the incorporation of data on runoff from the basins of 24 large rivers; the evaporation was calculated by Priestley–Taylor formula, and the water content were estimated with the use of Kalman filter. The correctness of the daily *ET* estimates for the global scale was checked by their comparison with the appropriate values from Princeton University product and MERRA databases. The former were obtained with the use of Penman–Monteith equation with incorporation of data from various satellites. The latter were based on the reanalysis data from GEOS-5 DAS NASA. The results of calculations for different months were used to construct maps of evaporation and transpiration for the globe. Analogous estimates of soil water content *W* in the root zone and evaporation, including a set of calculation results over 36 years (1980–2015) (v3a), were obtained in [90] with the use of a new (v3) version of GLEAM, containing the same input variables as the previous (v2) version of the model [94], also with the incorporation of satellite data. The version v3 used Priestley–Taylor formula, Kalman-filter algorithm, MOD44B package, and other products. For low vegetation, the root zone was considered in a two-layer variant (0–10, 10–100 cm), and for high vegetation, in a three-layer variant (0–10, 10–100, 100–250 cm). At a three-layer description, the water content were calculated with the use of finite-difference schemes for each horizon. New estimates of *W* and *ET* were obtained when modeling based on the data of measurements of various passive and active microwave sensors in C- and L-ranges of ESA CCI (for the set of results over 2003–2015, v3b) and data of SMOS satellite (for an analogous set over 2011–2015, v3c). The adequacy of the estimates of *W* and *ET* from sets v3a, v3b, and v3c is confirmed by their comparison with the measurement results of 2325 soil moisture sensors and fluxes at 91 flux towers by vortex covariation method for various types of LS. The comparison of *W* estimates from data sets showed their quality to be higher than that of analogous estimates from v2. All-weather satellite data in microwave range with a high resolution (100 m) were used in GLEAM to evaluate the *ET* and SSH for the Netherlands, Flanders, and West Germany [89]. SSH and *LST* were evaluated at a lesser scale with the use of LPRM model using measurements of AMSR-2 radiometer on GCOM-W1 satellite. The surface moisture content was also determined by the data of scatterometer ASCAT/Metop-A, -B. The water content in the root zone *W* were calculated with the use of a multilayer water balance model—a part of GLEAM, based on the observations of precipitation with assimilation of data on SSH. The datasets that enter the used version of GLEAM included estimates of potential *ET* from water surface, low and high vegetation, and bare soil with the use of Penman–Monteith equations and Priestley–Taylor constants. The data on short- and long-wave radiation were obtained from measurements of radiometer SEVIRI/Meteosat with resolution of 5 km, as well as from EUMETSAT LSA-SAF archive; the data on albedo were taken from measurements of MODIS/Terra and Aqua with 500-m resolution once in 16 days (MCD43A3 package). SSH estimates were compared with in-situ measurements at 29 sites in the examined territories, the mean coefficient of correlation was 0.76. The comparison of *ET* estimates obtained with the use of GLEAM with LSA SAF data revealed difference between them (coefficients of correlation of 0.65–0.95) depending on the vegetation type—for woody vegetation, the errors were greater than those for grassy and shrubby vegetation because of the interception of water by plants, which was the dominant process. Combining the data obtained from passive (AMSR-E) and active (ASCAT) microwave satellite sensors and the use of a developed technology [85] gave more accurate estimates of SSH for a soil layer with a depth up to 10 cm on a global scale. Such and analogous estimates, obtained with the use of Noah model (a component of GLDAS), were compared with the results of in-situ SSH measurements, taken from OZNET networks for the southeastern part of Australia, REMEDHUS for the central Spain, SMOSMANIA for the southern France, and CNR-IRP for Italy. These comparisons show that at a good correlation between both satellite products ($\underline{R} > 0.65$), their combining improves the time resolution of SSH estimates. In addition, the use of scaled estimates AMSR-E and ASCAT was found to be effective for regions with sparse or moderate vegetation. K. Zhang

et al. [159] showed that the accuracy of the daily estimate of soil water content based on the joint use of observation data on the brightness temperature from several satellites in the regime close to real time is higher than the accuracy of analogous estimates by data of each satellite. Estimates of soil moisture were based on the measurements of the brightness temperature by SMAP, SMOS, AMSR-2, FY3B, and FY3C equipment for the same day, followed by averaging these estimates to obtain their daily aggregate. The comparison of the combined estimates and those from each satellite with ground-based data from two networks in the Central Tibet and Anhui province (China) showed a noticeable increase in the accuracy of soil moisture estimates, especially in the second region. B. Zhu et al. [167] present a simplified algorithm for determining the moisture of bare soil surface with the use of measurements of L-range radiometers installed on SMOS and SMAP satellites. This algorithm consists of two parts: a model of surface radiation with dual polarization, which allows the effect of surface roughness to be reduced by using data on the reflectivity of the surface, and a model of soil moisture recovery, which utilizes the relationship between the corrected actual refractive index and the volumetric soil moisture content. In this approach, *SM* was determined with the incorporation of several available input characteristics: the brightness temperature of the microwave range at dual polarization, the surface temperature, and the content of sand and clay in the surface (0–10 cm) soil layer. The obtained estimates showed good agreement with the *SM* values calculated with the use of an appropriate integral equation (the *RMSE* values were <3% at all angles of incidence). The subsequent test of the algorithm with data of four-year experiments with radiation in L-range, carried out in BARC, yielded RMSE of 4.3 and 3.4% at the angles of incidence of 40° and 50°, respectively. The algorithm also showed a high efficiency for radiometers in L-range with larger angles of incidence installed on SMAP.

Estimation of Soil Surface Moisture Using Neural Networks

SSH estimates by satellite data can be also obtained with the use of neural networks NN [100, 121, 156]. N.J. Rodríguez-Fernández et al. [121] choose this set of estimates by SMOS data as a reference in learning NN to obtain a global nonlinear dependence (search for global nonlinear regression), relating the brightness temperatures T_{br}, measured by AMSR-E radiometer, with SMOS data set over the period of simultaneous mission of 1.5 year, after which the constructed network was used to evaluate SSH by the earlier AMSR-E observations. The sensitivity of T_{br} AMSR-E to changes in soil temperature was evaluated with the use of information from databases ERA-Land and MERRA-Land. One of the articles, where data of C- and X-ranges AMSR-E and information about soils was used, was chosen to obtain SSH estimates over 2003–2011. This set of estimates showed small biases (<0.02 m^3/m^3) and standard deviations (<0.04 m^3/m^3) from SMOS data over most of the world surface. SSH estimates from this set, as well as from sets AMSR-E, SM CCI, MERRA-Land, and ERA-Land were compared with many in-situ measurement results on four continents. A good agreement with field data was obtained for Australia, the results of calculations were found acceptable for Europe, mountain regions of the North America, and, to a much lesser extent, to the Sahel region. They also demonstrated considerable errors for regions of tropic and boreal forests. A similar approach was implemented in [156], where backpropagation neural networks BPNN were used to reconstruct a long time series of SSH values with the use of satellite-based estimates of the microwave vegetation index *MVI*. Here, BPNN training for each grid pixel was carried out for two years with the use of data on SSH from SMOS of level 3 (SMOSL3sm) as a training objective, taking into account the reflection indices R_s within ranges C/X/Ku/Ka /Q, as well as *MVI* from the data of radiometers AMSR-E and AMSR-2 as input characteristics, where *MVI* was used for correction for the effect of vegetation. In this case, the values of R_s and *MVI* were determined from the relationships with the brightness temperature T_{br}, measured by AMSR-E and AMSR-2. The training accuracy of the networks was evaluated by comparing the SSH values obtained with the use of BPNN (NN sm) with SMOSL3sm within the training period BPNN, by correlation coefficients (~0.67), bias (~–0.0005 m^3/m^3) and the root-mean-square error RMSE (~0.055 m^3/m^3). Good results at a global scale were obtained for Australia, the central part of USA, and Central Asia. The trained networks were used to construct for each pixel, according to AMSR-E data, global SSH time series over period 2003–2015, after which the products NN sm were evaluated by comparison with in-situ SSH observation data in all fragments of SCAN network. K. Muzalevskiy et al. [100] substantiated the possibility to evaluate the moisture content of bare soil surface with the help of NN, using radar data from Sentinel-1B satellite. Here, NN were considered as a means to construct a regression relationship between the backscatter coefficients, determined in Sentinel measurements, and polarimetric scatter characteristics, i.e., the anisotropy and entropy, and the reflectivity of SSH. The moisture and roughness of the soil surface are the main characteristics that affect this coefficient [106]). The required moisture values were determined using the obtained data on the reflecting capacity of soil. Estimates of the moisture content of the surface (0–5 cm) soil layer with the use of the proposed method for an agricultural field out of crop with bare soil in a village in Krasnoyarsk Krai, RF, yielded a

root-mean-square error ≥3% and a coefficient of determination ≤0.726 [100].

Estimates of Soil Moisture for Drought Conditions

In studies [78, 146], *SM* was evaluated based on its relationship with the water deficiency index *WDI* and precipitation. *WDI* was calculated as a combination of differences between the temperatures of LS and air, obtained with the use of their dependence on the projective cover (*LST*~*VI*), determined using MODIS data, in the form of a trapezoid with vortices corresponding to dry and saturated bare soil, vegetation in the state of water stress, and well moistened. These differences were constructed for each pixel using the energy balance equation, where the fluxes of latent and sensible heat fluxes were calculated with the use of data on meteorological characteristics, including air temperature, solar radiation, wind speed, and specific moisture content, the results of calculation of the surface and aerodynamic resistances, as well as MODIS data on albedo and *LAI*. The calculated values of temperature differences were used to determine the boundaries of a trapezoid for the dry and wet state of LS. The values of meteorological characteristics in [146] were derived from the data of direct measurements at weather stations, and those in [78] were loaded from CLDAS database. At the approach used in the study, the root-mean-square error of soil moisture estimate relative to measurements at different depths varied within 0.067–0.079 m^3/m^3. Variations in SSH at a global scale over the recent 40 years were analyzed by data ESA CCI (for the layer 0–5 cm), GLDAS-Noah (for the layer 0–10 cm), and ERA-Interim (for the layer 0–7 cm), the latter were closest to the measured values [38]. The authors note an appreciable decrease in the global averages of SSH in 1979–2017 and an increase in the downward trend in 2001–2017, illustrating them by global SSH maps. Drying was observed in sols with the seven main land use types, the largest proportion among them (~80%) being recorded in urban areas. At the same time, in 65% of cases of soil drying, it was due to an increase in temperature, while in 82% of moistening cases, due to the joint effect of temperature, precipitation, and an increase in vegetation area, characterized by *NDVI*. Under the condition of global warming, the area of soil drying in 1979–2017 increased at a rate of 1% per year. N. Nicolai-Shaw et al. [104] obtained quantitative estimates of the relationship between soil moisture *SM* during draught, determined by satellite data, and the temperature, precipitation, evapotranspiration, and plant characteristics at a peak of vegetation period for a global scale. The values of *SM* were obtained by data of ESA-CCI and ERA-Interim/Land; the values of evapotranspiration *ET*, by GLEAM data, and the values of temperature and precipitation, by data of ERA-Interim (ERA-Tx and ERA-P) (all values with a resolution of 0.25°, at a daily basis, over more than 30 years), the values of *NDVI*, by AVHRR/NOAA data with a resolution of (1/12)° once in two weeks, the values of *LAI* and *PAR*, by MODIS data with a resolution of 1 km once in 8 days, and the data on the degree of coverage by plants, by data of ESA CCI. The values of *SM* at drought, determined by satellite data from ESA CCI, were compared with analogous values obtained using ERA-Interim data and with the use of LSM and data of multi-frequency radiometer on the precipitation index *SPI* for the territories of all continents. For different parts of these territories, for drought peaks, specific features of the relationships between *SM* and the temperature, precipitation, the values of *ET* and the vegetation area were described. This approach enables monitoring droughts at large space and time scales with the use of satellite data. Note that, to analyze the long-term dynamics of water, energy, and carbon cycles over land surface, the European Space Agency ESA, under its program CCI in 2012, made available the first long-term set of global satellite data on soil moisture SM, ESA CCI SM. This set combined various active and passive microwave products of soil moisture, formed with the use of a single sensor, into three harmonized products—joined active, passive, and combined active + passive microwave products [40]. Compared with the first issue of this set, the latest (as of 2019) version ESA CCI *SM* contains many improvements along with data of several new satellite sensors with the expansion of its time coverage up to the interval 1978–2018 [53]. W. Wie et al. [148] used ERS data to develop a drought index *TVPDI*, which, in the authors' opinion, is a better indicator of land surface drying than those associated with the amount of precipitation *P*—the temperature *LST*, and with the state of vegetation—soil moisture *SM* (because of the interaction between the likely causes of draughts mentioned above). The possibility to use this index was substantiated based on its comparison with data on *SM*, *P*, *NDVI*, *LST*, other aridity indices, as well as the crop yield per unit area and the net primary production *NPP* (appropriate analysis was carried out for various space scales). *TVPDI* estimates at drought were more accurate than the results of the use of *P*, *NDVI*, and *LST*, in this case, the coefficient of correlation between *TVPDI* and *SM* was >0.64. *TVPDI* time series showed a good agreement over the space with other dryness indices and over time, with the crop yield per unit area and *NPP* for most regions of China. Estimates of *TVPDI* by MODIS data corresponded also to analogous estimates obtained with the use of Landsat data. As the result, the use of *TVPDI* for monitoring arid and humid areas in China made it possible to record noticeable space and time differences between the states of dryness–wetness on both monthly and annual scale.

Estimates of Soil Moisture Using New Promising Microwave Satellite Sensors

In the several recent years, integrated (airborne and surface) experiments were carried out to test microwave instruments planned for installation on new space platforms. Thus, study [164] is focused on SSH estimation based on measurement data from an airborne L-range microwave radiometer with synthesized aperture, which carried out earth surface sounding at variable incidence angles and planned for operation on satellites WCOM [135, 136] and TWRS [166]. T. Zhao et al. [164] studied the dependence of SSH estimates on these angles in algorithms corresponding to different polarizations, used to evaluate the brightness temperature and SSH, and in model LPRM; the effect of vegetation and LS roughness on the accuracy of those calculations was also estimated. These results were compared with the data of ground-based measurements of *SM* and the temperature; in this case, a range of angles was found for different polarizations, making it possible to obtain optimal SSH estimates. Publications [165, 166] present the results of analogous studies carried out to test the instruments for microwave L-range for TWRS satellite and aimed to increase the spatial resolution and the accuracy of SSH mapping by the joint use of the data of active and passive ERS in L-range [166], in L-, C-, and X-ranges [165], as well as data of the optical range. In both studies, SSH estimates for the 0–5 cm layer, obtained with the use of aircraft data of different resolutions (airborne radiometer and radar) for different sounding angles and frequencies, were compared with the results of ground-based measurements of soil moisture and temperature on two grids (in the basins of two rivers of Inner Mongolia (China)). High spatial variability was found in the values of both temperature and SSH for different types of land use (arable land, grain and grass vegetation) [166]. T. Zhao et al. [165] showed that difference between the brightness temperatures for the adjacent frequencies L- and C-, as well as C- and X-ranges are determined by the difference between SSH values, while the difference between the values of the brightness temperature at different angles of incidence are mostly due to the different moisture content of vegetation. In the authors' opinion, an increase in the number of observation channels leads to more reliable estimates of SSH at a resolution of L-band sensor of about 18 km.

Analysis of Possible Errors in Soil Moisture Estimates by Satellite Data

The difficulty in estimating soil moisture *SM* by high-resolution SAR data is mostly due to the need to provide accurate parameterization of soil roughness, to take into account the effect of the observation angle, and to ensure the continuity of the data. To use the existing sets of *SM* estimates by microwave data with a low resolution over a long time, for example, from ESA CCI SM web site, requires the use of scale-reducing algorithms to increase the spatial resolution of estimates from these sets. In addition to the data of such microwave measurements, the results of observations in VNIR ranges were used either to increase the scale of soil moisture estimates by microwave data or to directly determine its values. The advantages of VNIR range measurements are their very high resolution—both spatial (10 m for Sentinel-2) and temporal (less than a day for geostationary satellites) [113]. For example, S. Sabaghy et al. [122] discuss the results of SSH estimation by microwave data of SAR and radiometers of SMAP and SMOS satellites at a decrease in the scale, by data of VNIR ranges Landsat-8 OLI and MODIS, at the use of method of rediscretization (changes in the resolution of images in pixels), by data of airborne measurements with the use of PLMR radiometer and PLIS scatterometer under projects SMAPEx-4,-5 [157] and ground-based measurements in-situ and on OzNet network on the agricultural area Yanko in New South Wales (Australia).

Studying the specifics of errors in SSH estimates with the use of ERS data, carried out in [151], was aimed to improve the methods for optimal assimilation of such estimates in hydrological models. The authors considered the differences between time-invariant and daily errors in SSH estimates by ASCAT and SMAP measurements and analyzed the correlation between these daily errors and a quantitative estimate of plant biomass by leaf area index *LAI* and the amount of precipitation. In tropical regions, the difference between the time-invariant and daily errors is large in the dry season and small in the rain season. For the major portion of land surface, the daily errors show higher correlation with precipitation than with *LAI*. In areas with a low vegetation cover, including in barren lands, meadows, and open brushes, rain peaks coincide with peaks in the errors in SSH estimates, and the peaks in *LAI* values in all cases are attained after the passage of SSH error peaks. Thus, the time variations in the errors in soil moisture estimates is more due to precipitation than to variations in *LAI*.

An original method for estimating the moisture content of the surface soil layer with the use of GNSS navigation system is proposed in [81]. Taking into account the decrease in the amplitude of the beam refracted by soil, the authors constructed a polynomial regression relationship between the ratio of this amplitude to that of the incident beam and the moisture content of the surface (3.5 cm) layer and its temperature. The form of this relationship was determined by its calibration against measurement data of 18 satellites over 62 days out of the total of 241 days of measurements. The coefficient of correlation was 0.947, and the RMSE value was 0.013 cm^3/cm^3 (1.3%) at a scatter of SSH values between 0.272 and 0.489 cm^3/cm^3. This approach seems to require improvement, in particular,

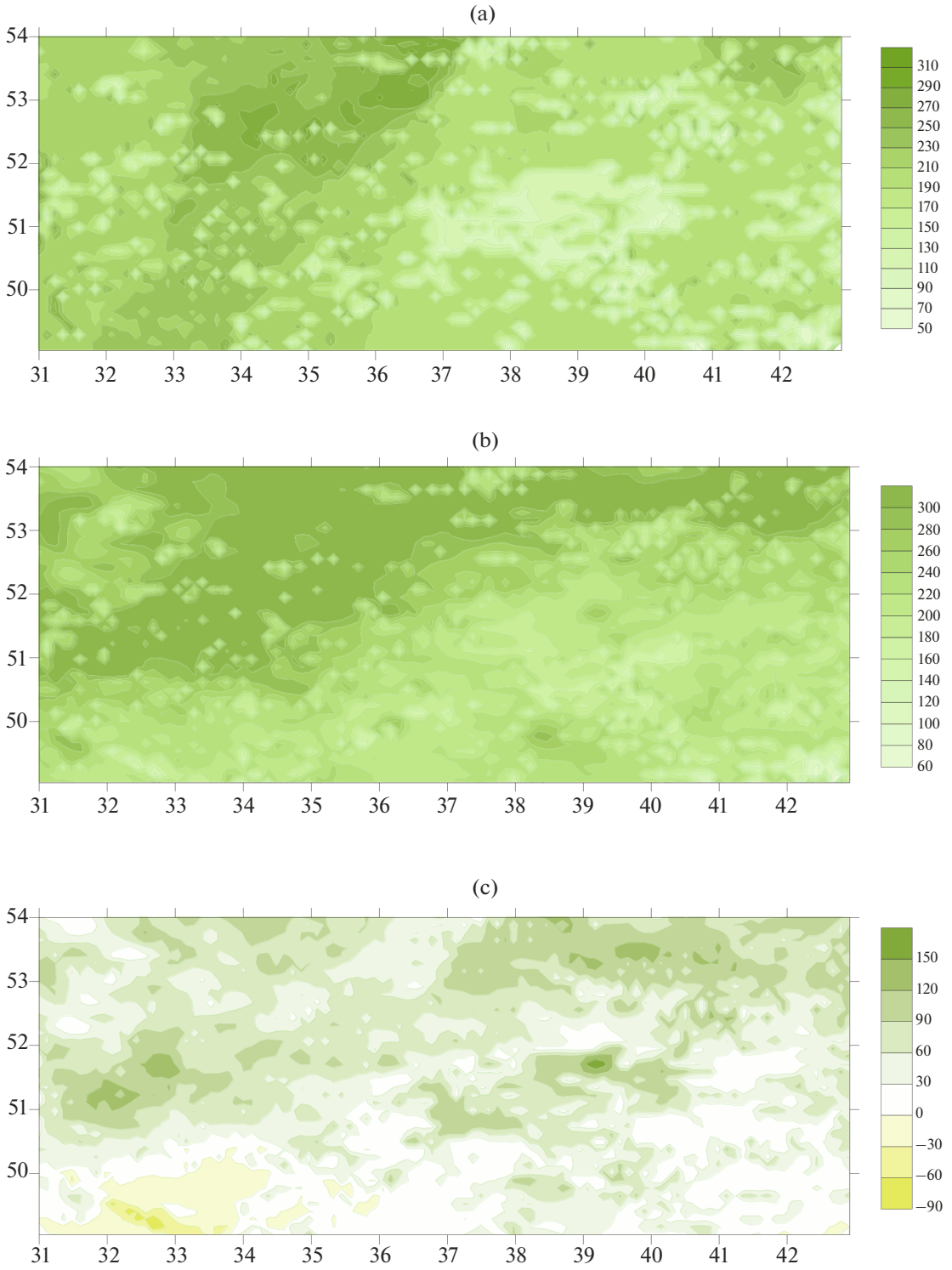

Fig. 2. Distribution of moisture storage in the 1-m soil layer in a part of Central Russia on August 22, 2017, calculated by the model (a) with the use of surface measurement data, (b) with initial soil moisture profile specified with the use of ASCAT data, and (c) their difference.

carrying out more measurements and detail verifying the accuracy of results.

CONCLUSIONS

The review gives the results of the use of ERS data

in different spectral ranges to evaluate the evapotranspiration and the soil surface humidity (SSH) and the moisture reserves of its active layer W as elements of the water and heat regimes of territories of different scales—from local to global. Under such approach, the article presents a retrospective of studies of the processes of water and heat exchange between land areas and the atmosphere (by implementing field hydrological–atmospheric experiments, regular collection of data on the LS and the surface layer of the atmosphere, and the development of models of these processes) since the mid-1980s until now. In addition, a review of databases of ground-based, satellite, and model data (global, regional, and local), accumulated in those studies, is given.

Considerable attention is paid in the study to the results of estimation of SSH and W with the incorporation of microwave range data, including those obtained with the use of SAR, as one of the most effectively developing lines of evaluating those values, which characterize the water availability in the examined territories. The results of application of such data under various physiographic conditions are analyzed. Estimates of the SSH, obtained with the use of neural networks, are given. The issues of the application of ERS data to estimating soil moisture content under drought conditions are considered.

The prospects of the development of satellite technologies for estimating LS and meteorological characteristics, used to calculate soil moisture content and other elements of water and heat regimes, are outlined, including the development of new high-resolution multispectral instrumentation, the construction of large databases, including cloud, methods of their treatment and assimilation in models. A brief description is given to a new promising line of obtaining remote sensing data with the use of numerous microsatellites of small size and weight with high-resolution sensors in either VNIR or microwave ranges. These microsatellites show a high (several times a day) recurrence.

The presented review can be used by researchers focused on simulating the processes of water and heat exchange in territories of different natural zones and obtaining estimates of soil water content and evaporation.

FUNDING

This study was carried out under Governmental Order to WPI RAS, Project 1–14, Subject FMWZ-2022-0001.

REFERENCES

1. Volkova, E.V., Estimates of the characteristics of cloud cover, precipitation, and hazardous weather phenomena by data of AVHRR radiometer with meteorological Earth satellites NOAA series round-the clock in automatic regime, *Sovrem. Probl. Dist. Zond. Zemli Kosm.*, 2013, vol. 10, no. 3, pp. 66–74.
2. Volkova, E.V., Determining precipitation totals based on data of SEVIRI/Meteosat-9,-10, and AVHRR/NOAA for European Russia, *Sovrem. Probl. Dist. Zond. Zemli Kosm.* 2014, vol. 11, no. 4, pp. 163–177.
3. Volkova, E.V. and Uspenskii, A.B., Estimates of cloud cover and precipitation characteristics by the data of scanning radiometers of polar-orbit and geosynchronous weather satellites, *Issled. Zemli Kosmosa*, 2015, no. 5, pp. 40–43.
4. Volkova, E.V. and Uspenskii, S.A., Remote determination of underlying surface temperature, surface air temperature, and effective temperature by satellite data for the southern European Russia, *Sovrem. Probl. Dist. Zond. Zemli Kosm.*, 2016, vol. 13, no. 5, pp. 291–303.
5. Kabeleva, Kh.A., ECOCLIMAP—A Database for the Surface Block ISBA in atmospheric models, *Uchen. Zap. Ros. Gidrometeorol. Univ.*, no. 3, pp. 54–60. http://elib.rshu.ru/files_books/pdf/3-5.pdf
6. Mitnik, L.M., Mitnik, M.L., and Zabolotskikh, E.V., Japanese satellite GCOM-W1: modeling, calibration, and first results of recovery of ocean and atmosphere parameters, *Sovrem. Probl. Dist. Zond. Zemli Kosm.*, 2013, vol. 10, no. 3, pp. 135–141.
7. Motovilov, Yu.G. and Startseva, Z.P., Numerical simulation of moisture exchange between active soil layer and the atmosphere, *Meteorol. Gidrol.*, 1985, no. 6, pp. 85–93.
8. Muzylev, E.L., Startseva, Z.P., Zeiliger, A.M., Ermolaeva, O.S., Volkova, E.V., Vasilenko, E.V., and Osipov, A.I., Using satellite data on land surface and weather characteristics in simulating water and thermal regimes of a large agricultural region, *Sovrem. Probl. Dist. Zond. Zemli Kosm.*, 2019, vol. 16, no. 3, pp. 44–60. https://doi.org/10.21046/2070-7401-2019-16-3-44-60
9. Muzylev, E.L., Startseva, Z.P., Uspenskii, A.B., Volkova, E.V., Vasilenko, E.V., Kukharskii, A.V., Zeiliger, A.M., and Ermolaeva, O.S., Using remote sensing data in simulating water and thermal regime of rural areas, *Sovrem. Probl. Dist. Zond. Zemli Kosm.*, 2017, vol. 14, no. 6, pp. 108–136.
10. Solov'ev, V.I., Uspenskii, A.B., and Uspenskii, S.A., Derivation of land surface temperature using measurements of IR radiances from geostationary meteorological satellites, *Russ. Meteorol. Hydrol.*, 2010, no. 3, pp. 159–167.
11. Uspenskii, A.B. and Shcherbina, G.I., Estimating land surface temperature and emissivity by measured outgoing thermal radiation from the NOAA satellite, *Issled. Zemli. Kosm.* 1996, no. 5. pp. 4–13.
12. Abid, N., Mannaerts, C., and Bargaoui, Z., Sensitivity of actual evapotranspiration estimation using the SEBS model to variation of input parameters (LST, DSSF, aerodynamics parameters, LAI, FVC), *ISPRS Geospatial Week, Enschede, Netherlands, 2019. The Intern. Archives of the Photogrammetry. Remote Sens. Spatial Inf.*

Sci., 2019, vol. XLII-2/W13, pp. 1193–1200. https://doi.org/10.5194/isprs-archives-XLII-2-W13-1193-2019

13. Anderson, M.C., Norman, J.M., Diak, G.R., Kustas, W.P., and Mecikalski, J.R., A two-source time-integrated model for estimating surface fluxes using thermal infrared remote sensing, *Remote Sens. Environ.*, 1997, vol. 60, no. 2, pp. 195–216.
14. Andre, J.-C., Goutorbe, J.-P., and Perrier, A., HAPEX-MOBLIHY: A Hydrologic Atmospheric Experiment for the Study of Water Budget and Evaporation Flux at the Climatic Scale, *Bull. Amer. Meteorol. Soc.*, 1986, vol. 67, no. 2, p. 138. https://doi.org/10.1175/1520-0477(1986)067<0138:HAHAEF>2.0.CO;2
15. Andreassian, V., Bergström, S., Chahinian, N., Duan, Q., Gusev, Ye.M., Littlewood, I., Machevet, T., Michel, C., Montanary, A., Moretti, G., Moussa, R., Nasonova, O.N., O'Connor, K., Paquet, E., Perrin, C., Rousseau, A., Schaake, J., Wagener, T., and Xie, Z., Catalogue of the Models Used in MOPEX 2004/2005, *Large Sample Basin Experiments for Hydrological Model Parameterization: Results of the Model Parameter Experiment—MOPEX*, Andreassian, V., Hall, A., Chahinian, N., Shaake, J., Wallingford, UK: IAHS Press, 2006, no. 307, pp. 41–93.
16. Angelini, L.P., Biudes, M.S., Machado, N.G., Geli, H.M.E., Vourlitis, G.L., Ruhoff, A., and de Souza Nogueira, J., Surface albedo and temperature models for surface energy balance fluxes and evapotranspiration using SEBAL and Landsat 8 over Cerrado-Pantanal, Brazil, *Sensors*, 2021, vol. 21, p. 7196. https://doi.org/10.3390/s21217196
17. Attema, E., Cafforio, C., Gottwald, M., Guccione, P., Monti-Guarnieri, A., Rocca, F., and Snoeij, P., Flexible dynamic block adaptive quantization for Sentinel-1 SAR missions, *IEEE Geosci. Remote Sens. Lett.*, 2010, vol. 7, no. 4, pp. 766–770.
18. Attema, E., Snoeij, P., Monti-Guarnieri, A., Rocca, F., Guccione, P., D'Aria, D., Croci, R., and Olanda, A., Sentinel-l Flexible Dynamic Block Adaptive Quantizer, *Conference Paper. EUSAR 2010*, Aachen, Germany, 2010, pp. 344–349. https://www.researchgate.net/publication/224233683
19. Bartalis, Z., Wagner, W., Naeimi, V., Hasenauer, S., Scipal, K., Bonekamp, H., Figa, J., and Anderson, C., Initial soil moisture retrievals from the METOP-A Advanced Scatterometer (ASCAT), *Geophys. Res. Lett.*, 2007, vol. 34, no. 20, L20401. https://doi.org/10.1029/2007GL031088
20. Bastiaanssen, W.G.M., Menenti, M., Feddes, R.A., and Holtslag, A.A.M., A remote sensing surface energy balance algorithm for land (SEBAL), Pt 1, Formulation, *J. Hydrol.*, 1998, vol. 212–213, pp. 198–212.
21. Bastiaanssen, W.G.M., Pelgrum, H., Wang, J., Ma Y., Moreno, J.F., Roerink, G.J., and van der Wal, T., A remote sensing surface energy balance algorithm for land (SEBAL), Pt 2, Validation, *J. Hydrol.*, 1998, vol. 212–213, pp. 223–229.
22. Bezerra, B.G., Silva, B.B., Santos, C.A.C., and Bezerra, J.R.C., Actual evapotranspiration estimation using remote sensing: comparison of SEBAL and SSEB approaches, *Adv. Remote Sens.*, 2015, vol. 4, no. 3, pp. 234–247.
23. Biancamaria, S., Lettenmaier, D.P., and Pavelsky, T.M., The SWOT Mission and its capabilities for land hydrology, *Surv. Geophys.*, 2016, vol. 37, pp. 307–337.
24. *Biospheric Aspects of the Hydrological Cycle (BAHC). Operation Plan*, Rep. No. 27, Core Project Office. Berlin, Germany: Institut fűr Meteorologie, Freie Univ., Berlin, 1993, pp. 1–103.
25. Blyth, E.M., Arora, V.K., Clark, D.B., Dadson, S.J., De Kauwe, M.G., Lawrence, D.M., Melton, J.R., Pongratz, J., Turton, R.H., Yoshimura,K., and Yuan, H., Advances in land surface modelling, *Current Clim. Change Rep.*, 2021, vol. 7, pp. 45–71.
26. Bolle, H.J. Identification and observation of desertification processes with the aid of measurements from space: Results from the European Field Experiment in Desertification-threatened Areas (EFEDA), *Desertification in Developed Countries*, Mouat, D.A., Hutchinson, S.F., Eds., Amsterdam, Netherlands: Kluwer Acad. Publ., 1995, p. 93–101. https://doi.org/10.1007/978-94-009-1635-7_7
27. Bolle, H.J., André, J.C., Arrue, J.L., Barth, H.K., Bessemoulin, P., Brasa, A., de Bruin, H.A.R., Cruces, J., Dugdale, G., Engman, E.T., Evans, D.L., Fantechi, R., Fiedler, F., van de Griend, A., Imeson, A.C., Jochum, A., Kabat, P., Kratzsch, T., Lagouarde, J.P., Langer, I., Llamas, R., Lopez-Baeza, E., Melia Miralles, J., Muniosguren, L.S., Nerry, F., Noilhan, J., Oliver, H.R., Roth, R., Saatchi, S.S., Sanchez, Dias J., de Santa Olalla, M., Shuttleworth, W.J., Soegaard, H., Stricker, J., Thornes, J., Vauclin, M., and Wickland, D., EFEDA: European field experiment in a desertification-threatened area, *Ann. Geophysicae*, 1993, vol. 11, pp. 173–189.
28. Brocca, L., Hasenauer, S., Lacava, T., Melone, F., Moramarco, T., Wagner, W., Dorigo, W., Matgen, P., Martínez-Fernández, J., Llorens, P., Latron, J., Martin, C., and Bitte, M., Soil moisture estimation through ASCAT and AMSR-E sensors: An intercomparison and validation study across Europe, *Remote Sens. Environ.*, 2011, vol. 115, no. 12, pp. 3390–3408.
29. Brown de Colstoun, E.C., Defries, R.S., and Townshend, J.R.G., Evaluation of ISLSCP Initiative II satellite-based land cover datasets and assessment of progress in land cover data for global model, *J. Geophys. Res.*, 2006, vol. 111, D22S07. https://doi.org/10.1029/2006JD007453
30. Brun, P., Zimmermann, N.E., Hari, C., Pellissier, L., and Karger, D.N., Global climate-related predictors at kilometer resolution for the past and future, *Earth Syst. Sci. Data*, 2022, vol. 14, pp. 5573–5603. https://doi.org/10.5194/essd-14-5573-2022
31. Burek, P., van der Knijff J., and de Roo, A., *LISFLOOD—Distributed Water Balance and Flood Simula-*

tion Model. Revised User Manual 2013, JCR Technical Report EUR 26162, Luxembourg: Luxembourg Publ. Office Eur. Union, 2013. 142 P. JRC78917. https://doi.org/10.2788/24982

32. Cammalleri C., Anderson M.C., Gao F., Hain C.R., Kustas W.P., Mapping daily evapotranspiration at field scales over rainfed and irrigated agricultural areas using remote sensing data fusion, *Agric. Forest Meteorol.*, 2014, vol. 186, pp. 1–11.
33. Cenci, L., Soil moisture-data assimilation for improving flash flood predictions in Mediterranean catchments. Case study: ASCAT and Sentinel 1 derived products, *Ph. D Thesis*, Pavia: Scuola Universitaria Superiore IUSS, 2016, Pavia, p. 123.
34. Cenci, L., Laiolo, P., Gabellani, S., Campo, L., Silvestro, F., Delogu, F., Boni, G., and Rudari, R., Assimilation of H-SAF soil moisture products for flash flood early warning systems. Study case: Mediterranean catchments, *IEEE J. Select. Topics Appl. Earth Observ. Rem. Sens.*, 2016, vol. 9, no. 12, pp. 5634–5646. https://doi.org/10.1109/JSTARS.2016.2598475
35. Chen, F., *The Noah Land Surface Model in WRF. A short tutorial*, LSM Group Meeting, 2007. NCAR, RAL, TIIMES, 2007. https://www.atmos.illinois.edu/~snesbitt/ATMS597R/notes/noahLSM-tutorial.pdf
36. Cooley, S.W., Ryan, J.C., and Smith, L.C., Human alteration of global surface water storage variability, *Nature*, 2021, vol. 591, pp. 78–81. https://doi.org/10.1038/s41586-021-03262-3
37. Dai, A., Historical and future changes in streamflow and continental runoff: natural and human-induced impacts: a review, *Terrestrial Water Cycle and Climate Change*, Tang, Q., Oki, T., *Geophysical Monograph Ser.*, Wiley, 2016, chapter 2, pp. 17–37. https://doi.org/10.1002/9781118971772.ch2
38. Deng, Y., Wang, S., Bai, X., Luo, G., Wu, L., Cao, Y., Li, H., Li, C., Yang, Y., Hu, Z., and Tian, S., Variation trend of global soil moisture and its cause analysis, *Ecol. Indicators*, 2020, vol. 110, 105939. https://doi.Org/10.1016/j.ecolind.2019.105939
39. Dickinson, R.E., Modeling evapotranspiration for three-dimensional global climate models, *Climate Processes and Climate Sensitivity*, Hanson, J.E., Takahashi, T., Geophys. Monogr. Ser. Amer. Geophys. Union., Washington, D. C., USA, 1984, vol. 29, pp. 58–72.
40. Dorigo, W., Wagner, W., Albergel, C., Albrecht, F., Balsamo, G., Brocca, L., Chung, D., Ertl, M., Forkel, M., Gruber, A., Haas, E., Hamer, P.D., Hirschi, M., Ikonen, J., de Jeu, R., Kidd, R., Lahoz, W., Liu, Y.Y., Miralles, D., Mistelbauer, T., Nicolai-Shaw, N., Parinussa, R., Pratola, C., Reimer, C., van der Schalie, R., Seneviratne, S.I., Smolander, T., and Lecomte, P., ESA CCI soil moisture for improved earth system understanding: state-of-the art and future directions, *Remote Sens. Environ.*, 2017, vol. 203, pp. 185–215. https://doi.org/10.1016/j.rse.2017.07.001
41. Dorigo, W.A., Wagner, W., Hohensinn, R., Hahn, S., Paulik, C., Xaver, A., Gruber, A., Drusch, M., Mecklenburg, S., van Oevelen, P., Robock, A., and Jackson, T., The International Soil Moisture Network: a data hosting facility for global in situ soil moisture measurements, *Hydrol. Earth Syst. Sci.*, 2011, vol. 15, pp. 1675–1698. https://doi.org/10.5194/hess-15-1675-2011
42. Duan, Q., Schaake, J., Andreassian, V., Franks, S., Goteti, G., Gupta, H.V., Gusev, Y.M., Habets, F., Hall, A., Hay, L., Hogue, T., Huang, M., Leavesley, G., Liang, X., Nasonova, O.N., Noilhan, J., Oudin, L., Sorooshian, S., Wagener, T., and Wood, E.F., Model Parameter Estimation Experiment (MOPEX): An overview of science strategy and major results from the second and third workshops, *J. Hydrol.*, 2006, vol. 320, pp. 3–17.
43. Durand, M., Gleason, C.J., Garambois, P.A., Bjerklie, D., Smith, L.C., Roux, H., Rodriguez, E., Bates, P.D., Pavelsky, T.M., Monnier, J., Chen, X., Di Baldas-sarre, G., Fiset, J.-M., Flipo, N., Frasson, R.P.d.M., Fulton, J., Goutal, N., Hossain, F., Humphries, E., Minear, J.T., Mukolwe, M.M., Neal, J.C., Ricci, S., Sanders, B.F., Schumann, G., Schubert, J.E., and Vilmin, L., An intercomparison of remote sensing river discharge estimation algorithms from measurements of river height, width, and slope, *Water Resour. Res.*, 2016, vol. 52, pp. 4527–4549. https://doi.org/10.1002/2015WR018434
44. Entekhabi, D., Njoku, E.G., O'Neill, P.E., Kent, H. Kellogg, K.H., Crow, W.T., Edelstein, W.E., Entin, J.K., Goodman, S.D., Jackson, T.J., Johnson, J., Kimball, J., Piepmeier, J.R., Koster, R.D., Martin, N., McDonald, K.C., Moghaddam, M., Moran, S., Reichle, R., Shi, J.C., Spencer, M.W., Thurman, S.W., Tsang, L., Van Zyl, J., The Soil Moisture Active Passive (SMAP) mission, *Proc. IEEE*, 2010, vol. 98, no. 5, pp. 704–716.
45. *FAO/IIASA/ISRIC/ISS-CAS/JRC, Harmonized World Soil Database (version 1.2)*, Rome-Laxenburg: FAO, 2012.
46. Faroux, S., Kaptué Tchuenté, A.T., Roujean, J.-L., Masson, V., Martin, E., Le Moigne, P., ECOCLIMAP-II/Europe: a twofold database of ecosystems and surface parameters at 1-km resolution based on satellite information for use in land surface, meteorological and climate models, *Geosci. Model Dev.*, 2013, no. 6, pp. 563–582. https://doi.org/10.5194/gmd-6-563-2013
47. Fernández-Long, M.E., Spescha, L., Barnatán, I., and Murphy, G., Modelo de balance hydrológico operative para el agro (BHOA). Rev., *Agronomía Ambiente. Buenos Aires, Argentina: Facultad de Agronomia UBA*, 2012, vol. 32, no. 1–2, pp. 31–47.
48. Fisher, R.A. and Koven, C.D., Perspectives on the future of land surface models and the challenges of representing complex terrestrial systems, *J. Adv. Model. Earth Syst.*, 2020, vol. 12, no. 4. e2018MS001453. https://doi.org/10.1029/2018MS001453

49. French, A.N., Hunsaker, D.J., and Thorp, K.R., Remote sensing of evapotranspiration over cotton using the TSEB and METRIC energy balance models, *Rem. Sens. Environ.*, 2015, vol. 158, pp. 281–294.

50. Global Climate Observing System (GCOS). https://gcos.wmo.int/en/home

51. Goutorbe, J.P., Lebel, T., Dolman, A.J., Gash, J.H.C., Kabat, P., Kerr, Y.H., Monteny, B., Prince, S.D., Stricker, J.N.M., Tinga, A., and Wallace, J.S., An overview of HAPEX-Sahel: a study in climate and desertification, *J. Hydrol.*, 1997, vol. 188–189, pp. 4–17. https://doi.org/10.1016/S0022-1694(96)03308-2

52. GRACE-FO. https://directory.eoportal.org/web/eoportal/satellite-missions/g/grace-fo

53. Gruber, A., Scanlon, T., van der Schalie, R., Wagner, W., and Dorigo, W., Evolution of the ESA CCI Soil Moisture climate data records and their underlying merging methodology, *Earth Syst. Sci. Data*, 2019, vol. 11, pp. 717–739. https://doi.org/10.5194/essd-11-717-2019

54. Häfliger, V., Martin, E., Boone, A., Ricci, S., and Biancamaria, S., Assimilation of synthetic SWOT river depths in a regional hydrometeorological model, *Water*, 2019, vol. 11, no. 1, p. 78.

55. Houser, P.R., De Lannoy, G.J.M., and Walker, J.P., Hydrologic data assimilation, *Approaches to Managing Disaster. Assessing Hazards, Emergencies and Disaster Impacts*, Tiefenbacher, J., Ed., Rijeka, Croatia: InTechOpen, 2012, Chapter 3, pp. 41–65.

56. H-SAF 2016. ASCAT H-SAF. http://hsaf.meteoam.it/. Accessed: March 24, 2016.

57. Huffman, G.J., Adler, R.F., Morrissey, M.M., Bolvin, D.T., Curtis, S., Joyce, R., McGavock, B., Susskind, J., Global precipitation at one-degree daily resolution from multi-satellite observations, *J. Hydrometeorol.*, 2001, vol. 2, pp. 36–50. https://doi.org/10.1175/1525-7541(2001)002<0036:GPAODD>2.0.CO;2g

58. Huffman, G.J. and Bolvin, D.T., Version 1.2. GPCP One-Degree Daily Precipitation Data Set Documentation. 2012. https://www.ncei.noaa.gov/pub/data/gpcp/daily-v1.2/documentation/1DD_v1.2_doc.pdf

59. Hutjes, R.W.A., Kabat, P., Running, S.W., Shuttleworth, W.J., Field, C., Bass, B., da Silva Dias, M.F., Avissar, R., Becker, A., Claussen, M., Dolman, A.J., Feddes, R.A., Fosberg, M., Fukushima, Y., Gash, J.H.C., Guenni, L., Hoff, H., Jarvis, P.G., Kayane, I., Krenke, A.N., Liu, C., Meybeck, M., Nobre, C.A., Oyebande, L., Pitman, A., Pielke, Sr. R.A., Raupach, M., Saugier, E.D., Schulze, E.D., Sellers, P.J., Tenhunen, J.D., Valentini, R., Victoria, R.L., and Vörösmarty, C.J., Biospheric aspects of the hydrological cycle, *J. Hydrol.*, 1998, vols. 212–213., no. 14, pp. 1–21.

60. ICESat2 mission. http://icesat.gsfc.nasa.gov/icesat2/.

61. ICESat2. https://directory.eoportal.org/web/eoportal/satellite-missions/i/icesat-2.

62. IGBP igbp.net.

63. ISD https://www.ncei.noaa.gov/products/land-based-station/integrated-surface-database

64. ISLSCP Initiative II Collection. Data set, Hall, F.G., Collatz, G.J., Meeson, B.W., Los, S.O., Brown De Colstoun, E., Landis, D.R., Oak Ridge, Tennessee, U.S.A: Oak Ridge National Laboratory Distributed Active Archive Center, 2011. http://daac.ornl.gov/.doi 10.3334/ORNLDAAC/1001

65. ISMN http://www.ipf.tuwien.ac.at/insitu

66. Karger, D.N., Conrad, O., Böhner, J., Kawohl, T., Kreft, H., Soria-Auza, R.W., Zimmermann, N.E., Linder, P., and Kessler, M., Climatologies at high resolution for the Earth land surface areas, *Sci. Data*, 2017, vol. 4, 170122. https://doi.org/10.1038/sdata.2017.122

67. Kawanishi, T., Sezai, T, Ito, Y., Imaoka, K., Takeshima, T., Ishido, Y., Shibata, A., Miura, M., Inahata, H., and Spencer, R.W., The Advanced AMSR-E. NASDA's contribution to the EOS for Global Energy and Water Cycle Studies, *IEEE Trans. Geosci. Remote Sens.*, 2003, vol. 41, pp. 184–194.

68. Kerr, Y.H., Imbernon, J., Dedieu, G., Hautecoeur, O., Lagouarde, J.-P., and Seguin, B., NOAA AVHRR and Its Uses for Rainfall and Evapotranspiration Monitoring, *Int. J. Remote Sens.*, 1989, vol. 10, pp. 847–854. https://doi.org/10.1080/01431168908903925

69. Kerr, Y.H., Waldteufel, P., Wigneron, J.P., Delwart, S., Cabot, F., Boutin, J., Escorihuela, M.-J., Font, J., Reul, N., Gruhier, C., Juglea, S.E., Drinkwater, M.R., Hahne, A., Martin-Neira, M., and Mecklenburg, S., The SMOS Mission: New tool for monitoring key elements of the global water cycle, *Proc. IEEE*, 2010, vol. 98, no. 5, pp. 666–687.

70. Krenke, A.N., Green, A.M., and Georgiadi, A.G., 1990, KUREX-88 – Hydrology in Atmospheric Processes Experiment, *Proc. Ljubljana Symp. IAHS Publ.*, 1990, no. 191, pp. 5.1–5.17.

71. Kuchment, L.S. and Startseva, Z.P., Sensitivity of evapotranspiration and soil moisture in wheat fields to changes in climate and direct effects of carbon dioxide, *Hydrol. Sci. J.*, 1991, vol. 36, no. 6, pp. 631–643.

72. KUREX-91, Goel, N.S., Kozoderov, V., and Deering, D., *Rem. Sens. Rev.*, Amsterdam, Netherlands: Harwood Acad. Publ., 1998, vol. 17, nos. 1–4.

73. Laiolo, P., Gabellani, S., Campo, L., Cenci, L., Svestro, F., Delogu, F., Boni, G., Rudari, R., Puca, S., and Pisani, A.R., Assimilation of remote sensing observations into a continuous distributed hydrological model: impacts on the hydrological cycle, *Conference Paper. IGARSS-2015*, New York, USA: IEEE Publisher, 2015. https://doi.org/10.1109/IGARSS.2015.7326015

74. Landsat https://www.usgs.gov/landsat-missions/landsat-data-access

75. Landsat-9 https://landsat.gsfc.nasa.gov/data/

76. Landsat 9. Data Users Handbook. Version 1.0. February 2022. LSDS-2082, Sioux Falls, South Dakota, USA: EROS Center, 2022.

77. LCD https://www.ncei.noaa.gov/products/land-based-station/local-climatological-data

78. Leng, P., Li, Z.-L., Duan, S.-B., Gao, M.-F., and Huo, H.-Y., A practical approach for deriving all-weather soil moisture content using combined satellite and meteorological data, *ISPRS J. Photogrammetry Remote Sens.*, 2017, vol. 131, pp. 40–51. https://doi.org/10.1016/j.isprsjprs.2017.07.013

79. Levizzani, V. and Cattani, E., Satellite remote sensing of precipitation and the terrestrial water cycle in a changing climate, *Remote Sens.*, 2019, vol. 11, no. 19. pp. 2301.

80. Li, X., Xin, X., Peng, Z., Zhang, H., Li, L., Shao, S., and Liua, Q., Estimation of land surface heat fluxes based on visible infrared imaging radiometer suite data: case study in northern China, *J. Appl. Rem. Sens.*, 2017, vol. 11, no. 4. 046012. https://doi.org/10.1117/1.JRS.11.046012

81. Li, Y., Yu, K., Li, J., Jin, T., Chang, X., Zhang, Q., and Yang, S., Measuring soil moisture with refracted GPS signals, *IEEE Geosci. Remote Sens. Lett.*, 2022. https://doi.org/10.1109/LGRS.2022.3161409

82. Li, Z., Liu, X., Ma, T., Kejia, D., Zhou, Q., Yao, B., and Niu, T., Retrieval of the surface evapotranspiration patterns in the alpine grassland–wetland ecosystem applying SEBAL model in the source region of the Yellow River, China, *Ecol. Model.*, 2013, vol. 270, pp. 64–75. https://doi.org/10.1016/j.ecolmodel.2013.09.004

83. Liang, S., Cheng, C., Jia, K., Jiang, B., Liu, Q., Xiao, Z., Yao, Y., Yuan, W., Zhang, X., Zhao, X., and Zhou, J., The Global LAnd Surface Satellite (GLASS) products suite, *Bull. Amer. Meteorol. Soc.*, 2020. https://doi.org/10.1175/BAMS-D-18-0341.1

84. Liang, S., Zhao, X., Liu, S., Yuan, W., Cheng, X., Xiao, Z., Zhang, X., Liu, Q., Cheng, J., Tang, H., Qu, Y., Bo, Y., Qu, Y., Ren, H., Yu, K., and Townshend, J., A long-term Global LAnd Surface Satellite (GLASS) data-set for environmental studies, *Intern. J. Digital Earth*. https://doi.org/10.1080/17538947.2013.805262

85. Liu, Y.Y., Parinussa, R.M., Dorigo, W.A., De Jeu, R.A.M., Wagner, W., van Dijk, A.I.J.M., McCabe, M.F., and Evans, J.P., Developing an improved soil moisture dataset by blending passive and active microwave satellite-based retrievals, *Hydrol. Earth Syst. Sci.*, 2011, vol. 15, pp. 425–436. https://doi.org/10.5194/hess-15- 425-2011

86. López, O., Houborg, R., and McCabe, M.F., Evaluating the hydrological consistency of evaporation products using satellite-based gravity and rainfall data, *Hydrol. Earth Syst. Sci.*, 2017, vol. 21, no. 1, pp. 323–343. www.hydrol-earth-syst-sci.net/21/323/2017/. https://doi.org/10.5194/hess-21-323-2017

87. Loveland, T.R., Reed, B.C., Brown, J.F., Ohlen, D.O., Zhu, Z., Yang, L., and Merchant J.W., Development of a global landcover characteristics database and IGBP DISCover from 1 km AVHRR data, *Int. J. Remote Sens.*, 2000, vol. 21, pp. 1303–1330.

88. Mallick, K., Toivonen, E., Trebs, I., Boegh, E., Cleverly, J., Eamus, D., Koivusalo, H., Drewry, D., Arndt, S.K., Griebel, A., Beringer, J., and Garcia, M., Bridging thermal infrared sensing and physically-based evapotranspiration modeling: from theoretical implementation to validation across an aridity gradient in Australian ecosystems, *Water Resour. Res.*, 2018, vol. 54, no. 5, pp. 3409–3435. https://doi.org/10.1029/2017WR021357

89. Martens, B, de Jeu, R.A.M., Verhoest, N.E.C., Schuurmans, H., Kleijer, J., and Miralles, D.G., Towards estimating land evaporation at field scales using GLEAM, *Remote Sens.*, 2018, vol. 10, no. 11, pp. 1720. https://doi.org/10.3390/rs10111720

90. Martens, B., Miralles, D.G., Lievens, H., van der Schalie, R., de Jeu, R.A.M., Fernández-Prieto, D., Beck, H.E., Dorigo, W.A., and Verhoest, N.E.C., GLEAM v3: satellite-based land evaporation and root-zone soil moisture, *Geosci. Model Dev.*, 2017, vol. 10, pp. 1903–1925. www.geosci-model-dev.net/10/1903/2017/. https://doi.org/10.5194/gmd-10-1903-2017

91. Masson, V., Champeaux, J.-L., Chauvin, F., Meryguet, C., and Lacaze, R., A global database of land surface parameters at 1-km resolution in meteorological and climate models, *J. Clim.*, 2003, vol. 16, no. 9, pp. 1261–1282. https://doi.org/10.1175/1520-0442-16.9.1261

92. McCabe, M.F., Rodell, M., Alsdorf, D.E., Miralles, D.G., Uijlenhoet, R., Wagner, W., Lucieer, A., Houborg, R., Verhoest, N.E.C., Franz, T.E., Shi, J., Gao, H., and Wood, E.F., The future of Earth observation in hydrology, *Hydrol. Earth Syst. Sci.*, 2017, vol. 21., pp. 3879–3914.

93. Ménard, C.B., Ikonen, J., Rautiainen, K., Aurela, M., Arslan, A.N., Pulliainen, J., Effects of meteorological and ancillary data, temporal averaging, and evaluation methods on model performance and uncertainty in a land surface model, *J. Hydrometeorol.*, 2015, vol. 16, pp. 2559–2576. https://doi.org/10.1175/JHM-D-15-0013.1

94. Miralles, D.G., Holmes, T.R.H., de Jeu, R.A.M., Gash, J.H., Meesters, A.G.C.A., and Dolman, A.J., Global land-surface evaporation estimated from satellite-based observations, *Hydrol. Earth Syst. Sci.*, 2011, vol. 15, pp. 453–469. https://doi.org/10.5194/hess-15-453-2011

95. Miralles, D.G., de Jeu, R.A.M., Gash, J.H., Holmes, T.R.H., and Dolman, A.J., Magnitude and variability of land evaporation and its components at the global scale, *Hydrol. Earth Syst. Sci.*, 2011, vol. 15, pp. 967–981. https://doi.org/10.5194/hess-15-967-2011

96. Mitchell, K.E., Lohmann, D., Houser, P.R., Wood, E.F., Schaake, J.C., Robock, A., Cosgrove, B.A., Sheffield, J., Duan, Q., Luo, L., Higgins, R.W., Pinker, R.T., Tarpley, J.D., Lettenmaier, D.P., Marshall, C.H., Entin, J.K., Pan, M., Shi, W., Koren, V., Meng, J., Ramsay, B.H., and Bailey, A.A., The multi-institution North American Land Data As-

similation System (NLDAS): Utilizing multiple GCIP products and partners in a continental distributed hydrological modeling system, *J. Geophys. Res. Atm.*, 2004, vol. 109, Iss. D7. D07S9016. https://doi.org/10.1029/2003JD003823

97. MODIS ALBEDO http://modis-atmos.gsfc.nasa.gov/ALBEDO/index.html
98. MODIS NDVI http://modis-atmos.gsfc.nasa.gov/ECOSYSTEM/
99. Mu, Q., Zhao, M., and Running, S.W., Improvements to a MODIS global terrestrial evapotranspiration algorithm, *Remote Sens. Environ.*, 2011, vol. 115, pp. 1781–1800.
100. Muzalevskiy, K. and Zeyliger, A., Application of Sentinel-1B polarimetric observations to soil moisture retrieval using neural networks: case study for bare Siberian chernozem soil, *Remote Sens.*, 2021, vol. 13, 3480. https://doi.org/10.3390/rs13173480
101. Muzylev, E., Startseva, Z., Volkova, E., and Vasilenko, E., Utilizing satellite data of several spectral ranges for modeling the processes of water and heat regime formation of vast territories, *Sovrem. Probl. Dist. Zond. Zemli Kosm.*, 2020, vol. 17, no. 6, pp. 129–136. https://doi.org/10.21046/2070-7401-2020-17-6-129-136
102. NCEI products. https://www.ncei.noaa.gov/products
103. Ndou, N.N., Palamuleni, L.G., and Ramoelo A., Modelling depth to groundwater level using SEBAL-based dry season potential evapotranspiration in the upper Molopo River Catchment, South Africa, *Egypt. J. Rem. Sens. Space Sci.*, 2017. https://doi.org/10.1016/j.ejrs.2017.08.003
104. Nicolai-Shaw, N., Zscheischler, J., Hirschi, M., Gudmundsson, L., and Seneviratne, S.I., A drought event composite analysis using satellite remote-sensing based soil moisture, *Remote Sens. Environ.*, 2017, vol. 203, pp. 216–225. https://doi.org/10.1016/j.rse.2017.06.014
105. Niu, G.Y., Yang, Z.L., Mitchell, K.E., Chen, F., Ek, M.B., Barlage, M., Kumar, A., Manning, K., Niyogi, D., Rosero, E., Tewari, M., and Xia, Y., The community Noah land surface model with multiparameterization options (Noah-MP) 1. Model description and evaluation with local scale measurements, *J. Geophys. Res.*, 2011, vol. 116. D12109. https://doi.org/10.1029/2010JD015139
106. Oh, Y., Sarabandi, K., and Ulaby, F.T., An empirical model and an inversion technique for radar scattering from bare soil surfaces, *IEEE Trans. Geosci. Remote Sens.*, 1992, vol. 30, no. 2, pp. 370–381.
107. Oki, T., Imaoka, K., and Kachi, M., AMSR Instruments on GCOM-W1/2: concepts and applications, *IEEE IGARSS-10. Honolulu, Hawaii, New York, USA: IEEE Publ.*, 2010. http://vigir.missouri.edu/~gdesouza/Research/Conference_CDs/IGARSS_2010/pdfs/2907.pdf
108. O'Neill, K.P., Harden, J.W., Trumbore, S.E., Bentley, M.O., Winston, G., Stephens, B.B., and Black, T.A., *Boreal Ecosystem-Atmosphere Study (BOREAS) 1993 Field Notes, Thompson, Manitoba, Open-File Report 95-488. U.S. Geol. Survey. U.S. Department of the Interior*, 66 p. https://doi.org/10.3133/ofr95488
109. OSCAR. https://www.wmo-sat.info/oscar/
110. Ottlé, C. and Vidal-Madjar, D., Assimilation of soil-moisture inferred from infrared remote sensing in a hydrological model over the HAPEX-MOBILHY Region, *J. Hydrol.*, 1994, vol. 158, pp. 241–264. https://doi.org/10.1016/0022-1694(94)90056-6
111. Overgaard, J., Rosbjerg, D., and Butts, M.B., Land-surface modeling in hydrological perspective—a review, *Biogeosciences*, 2006, vol. 3, pp. 229–41.
112. Panagos, P., Van Liedekerke, M., Jones, A., and Montanarella, L. European Soil Data Centre: Response to European policy support and public data requirements, *Land Use Policy*, 2012, vol. 29, no. 2, pp. 329–338. https://doi.org/10.1016/j.landusepol.2011.07.003
113. Peng, J., Albergel, C., Balenzano, A., Brocca, L., Cartus, O., Cosh, M.H., Crow, W.T., Dabrowska-Zielinska, K., Dadson, S., Davidson, M.W.J., de Rosnay, P., Dorigo, W., Gruber, A., Hagemann, S., Hirschi, M., Kerr, Y.H., Lovergine, F., Mahecha, M.D., Marzahn, P., Mattia, F., Musial, J.P., Preuschmann, S., Reichle, R.H., Satalino, G., Silgram, M., van Bodegom, P.M., Verhoest, N.E.C., Wagner, W., Walker, J.P., Wegmüller, U., and Loew, A., A roadmap for high-resolution satellite soil moisture applications—confronting product characteristics with user requirements, *Remote Sens. Environ.*, 2021, vol. 252, 112162. https://doi.org/10.1016/j.rse.2020.112162
114. Picoli, M.C.A., Simoes, R., Chaves, M., Santos, L.A., Sanchez, A., Soares, A., Sanches, I.D., Ferreira, K.R., Queiroz, G.R., CBERS Data Cube: A powerful technology for mapping and monitoring Brazilian biomes, *ISPRS Annals Photogrammetry, Remote Sens. Spatial Inform. Sci. V. V-3-2020. XXIV ISPRS Congress (2020 edition)*, pp. 533–539. https://doi.org/10.5194/isprs-annals-V-3-2020-533-2020
115. Pitman, A.J., The evolution of, and revolution in, land surface schemes designed for climate models, *Int. J. Clim.*, 2003, vol. 23, pp. 479–510.
116. Rains, D., Lievens, H., De Lannoy, G.J.M., McCabe, M., de Jeu, R.A.M., and Miralles, D.G., Sentinel-1 backscatter assimilation using support vector regression or the water cloud model at European soil moisture sites, *IEEE Geosci. Remote Sens. Lett.*, 2022, vol. 19, 4013105. https://doi.org/10.1109/LGRS.2021.3073484
117. Rautiainen, K., Parkkinen, T., Lemmetyinen, J., Schwank, M., Wiesmann, A., Ikonen, J., Derksen, C., Davydov, S., Davydova, A., Boike, J., Langer, M., Drusch, M., and Pulliainen, J., SMOS prototype algorithm for detecting autumn soil freezing, *Remote Sens. Environ.*, 2016, vol. 180, 346360. https://doi.org/10.1016/j.rse.2016.01.012
118. Reichle, R., Koster, R., De Lannoy, G., Crow, W., and Kimball, J., *SMAP Level 4 Surface and Root Zone Soil Moisture (L4_SM) Data Product*, Algorithm Theoretical Basis Document, Revision A. December 9. 2014. Greenbelt, MD, USA: NASA Goddard Space Flight Center, 2014. 66 p. https://smap.jpl.nasa.gov›272_L4_SM_RevA_web

119. Rodell, M., Famiglietti, J.S., Wiese, D.N., Reager, J.T., Beaudoing, H.K., Landerer, F.W., and Lo, M.-H., Emerging trends in global freshwater availability, *Nature*, 2018, May 31, vol. 557, pp. 651–659.

120. Rodell, M., Houser, P.R., Jambor, U., Gottschalk, J., Mitchell, K., Meng, C.-J., Arsenault, K., Cosgrove, B., Radakovich, J., Bosilovich, M., Entin, J.K., Walker, J.P., Lohmann, D., and Toll, D., The Global Land Data Assimilation System, *Bull. Am. Met. Soc.*, 2004, no. 3, pp. 381–394.

121. Rodríguez-Fernández, N.J., Kerr, Y.H., van der Schalie, R., Al-Yaari, A., Wigneron, J.-P., de Jeu, R., Richaume, P., Dutra, E., Mialon, A., Drusch, M., Long term global surface soil moisture fields using an SMOS-trained neural network applied to AMSR-E data, *Remote Sens.*, 2016, vol. 8, no. 11, p. 959. https://doi.org/10.3390/rs8110959

122. Sabaghy, S., Walker, J.P., Renzullo, L.J., Akbarn, R., Chan, S., Chaubell, J., Das, N., Dunbar, R.S., Entekhabi, D., Gevaert, A., Jackson, T.J., Loew, A., Merlin, O., Moghaddam, M., Peng, J.A., Peng, J.Z., Piepmeier J., Rüdiger C., Stefan V., Wu X., Ye N., Yueh S., Comprehensive analysis of alternative downscaled soil moisture products, *Remote Sens. Environ.*, 2020, vol. 239, 111586. https://doi.org/10.1016/j.rse.2019.111586

123. Schaake, J., Cong, S., and Duan, Q., The US MOPEX Data Set, *Large Sample Basin Experiments for Hydrological Model Parameterization: Results of the Model Parameter Experiment—MOPEX. IAHS Publ.*, no. 307, 2006, pp. 9–28.

124. Schmugge, T.J., Andre, J.-C., and Goutorbe, J.-P., HAPEX-MOBILHY: results from the special observing period, *Remote Sensing of the Biosphere. Proc. 1990 Tech. Symp. Optics, Electro-Optics, and Sensors (SPIE)*, Orlando, FL, USA, 1990, vol. 1300. https://doi.org/10.1117/12.21397

125. Schneider, R., Godiksen, P.N., Villadsen, H., Madsen, H., and Bauer-Gottwein, P., Application of CryoSat-2 altimetry data for river analysis and modeling, *Hydrol. Earth Syst. Sci.*, 2017, vol. 21, no. 2, pp. 751–764.

126. Seguin, B., Assad, E., Freteaud, J.-P., Imbernon, J., Kerr, Y.H., and Lagouarde, J.-P., Use of meteorological satellites for water balance monitoring in Sahelian Regions, *Int. J. Remote Sens.*, 1989, vol. 10, pp. 1101–1117. https://doi.org/10.1080/01431168908903948

127. Seguin, B., Lagouarde, J.-P., and Savane, M., The assessment of regional crop water conditions from meteorological satellite thermal infrared data, *Remote Sens. Environ.*, 1991, vol. 35, pp. 141–148. https://doi.org/10.1016/0034-4257(91)90007-S

128. Sellers, P.J., Canopy reflectance, photosynthesis and transpiration, *Int. J. Remote Sens.*, 1985, vol. 6, no. 8, pp. 1335–1372. https://doi.org/10.1080/01431168508948283

129. Sellers, P.J., Hall, F.G., Asrar, G., Strebel, D.E., and Murphy, R.E., The first ISLSCP field experiment (FIFE), *Bull. Am. Meteorol. Soc.*, 1988, vol. 69, no. 1, pp. 22–27.

130. Sellers, P.J., Hall, F.G., Asrar, G., Strebel, D.E., and Murphy, R.E., An overview of the first international satellite land surface climatology project (ISLSCP) Field Experiment (FIFE), *J. Geophys. Res.*, 1992, vol. 97, no. D17, pp. 18345–18371.

131. Sellers, P., Hall, F., Margolis, H., Kelly, B., Baldocchi, D., den Hartog, G., Cihlar, J., Ryan, M.G., Goodison, B., Crill, P., Ranson, K.J., Lettenmaier, D., and Wickland, D.E., The Boreal Ecosystem–Atmosphere Study (BOREAS): An overview and early results from the 1994 field year, *Bull. Amer. Meteorol. Soc.*, 1995, vol. 76, no 9, pp. 1549–1577. https://doi.org/10.1175/1520-0477(1995)076<1549:BESAO>2.0.CO;2

132. Sellers, P.J., Mintz, Y., Sud, Y.C., and Dalcher, A., A simple biosphere model (SiB) for use within general circulation models, *J. Atmos. Sci.*, 1986, vol. 43, no. 6, pp. 505–531.

133. Sellers, P.J., Rasool, S.I., and Bolle, H.J., A review of satellite data algorithms for studies of the land surface, *Bull. Am. Meteorol. Soc.*, 1990, vol. 71, no. 10, p. 1429–1447.

134. Serafini, Y.V., Estimation of the evapotranspiration using surface and satellite data, *Int. J. Remote Sens.*, 1987, vol. 8, pp. 1547–1562. https://doi.org/10.1080/01431168708954796

135. Shi, J., Dong, X., Zhao, T., Du, J., Jiang, L., Du, Y., Liu, H., Wang, Z., Ji, D., and Xiong, C., WCOM: The science scenario and objectives of a global water cycle observation mission, *Proc. IGARSS-2014. Quebec City, Canada; New York, USA: IEEE Publ.*, 2014, pp. 3646–3649. https://doi.org/10.1109/IGARSS.2014.6947273

136. Shi, J., Dong, X., Zhao, T., Du, Y., Liu, H., Wang, Z., Zhu, D., Ji, D., Xiong, C., and Jiang, L., The Water Cycle Observation Mission (WCOM): Overview, *Proc. IGARSS-2016, Beijing, China. New York, USA: IEEE Publ.*, 2016, pp. 3430–3433. https://doi.org/10.1109/IGARSS.2016.7729886

137. Shi, J., Zhao, T., Cui, Q., and Yao, P., Airborne and spaceborne passive microwave measurements of soil moisture, *Observation and Measurement of Ecohydrological Processes, Ecohydrology*, X. Li and Vereecken, H., Eds., Berlin, Heidelberg, Germany: Springer-Verlag GmbH, 2019, Chapter, pp. 71–105. https://doi.org/10.1007/978-3-662-48297-1_3

138. Shimoda, H., Murakami, H., Oki, T., Honda, Y., and Igarashi, T., Overview of GCOM, *Proc. IGARSS-2011. Vancouver, Canada. New York, USA: IEEE Publ.*, 2011, pp. 4134-4137. doi . http://www.grss-ieee.org/wp-content/uploads/2011/07/OverviewofGCOM.pdf https://doi.org/10.1109/IGARSS.2011.6050143

139. Spennemann, P.C., Fernández-Longm, M.E., Gattinoni, N.N., Cammalleri, C., and Naumann, G., Soil moisture evaluation over the Argentine Pampas using models, satellite estimations and in-situ measurements, *J. Hydrol. Regional Studies*, 2020, vol. 31, 100723, pp. 1–18.

140. Startseva, Z., Muzylev, E., Volkova, E., Uspensky, A., and Uspensky, S., Water and heat regimes modelling for a vast territory using remote-sensing data, *Int. J. Rem. Sens.*, 2014, vol. 35, no. 15, pp. 5775–5799. https://doi.org/10.1080/01431161.2014.945003

141. Stephens, G., Polcher, J., Zeng, X., van Oevelen, P., Poveda, G., Bosilovich, M., Ahn M.-H., Balsamo, G.,

Duan, Q., Hegerl, G., Jakob, C., Lamptey, B., Leung, R., Piles, M., Su, Z., Dirmeyer, P., Findell, K.L., Verhoef, A., Ek, M., L'Ecuyer, T., Roca, R., Nazemi, A., Dominguez, F., Klocke, D., and Bony, S., The first 30 years of GEWEX, *Bull. Amer. Meteorol. Soc.*, Nov. 2022, 66 p. https://doi.org/10.1175/BAMS-D-22-0061.1

142. Taconet, O., Bernard, L., and Vidal-Madjar, D., Evapotranspiration over agricultural region using a surface flux/temperature model based on NOAA-AVHRR data, *J. Clim. Appl. Meteorol.*, 1986, vol. 25, no. 3, pp. 284–307. https://doi.org/10.1175/1520-0450(1986)025<0284:EOAARU>2.0.CO;2
143. Tapley, B.D., Bettadpur, S., Watkins, M., and Reigber, C., The gravity recovery and climate experiment: Mission overview and early results, *Geophys. Res. Lett.*, 2004, vol. 31. L09607. doi . ftp://podaac.jpl.nasa.gov/allData/grace/L2/CSR/RL05/ https://doi.org/10.1029/2004GL019920
144. Tofigh, S., Rahimi, D., and Zakerinejad, R., A comparison of actual evapotranspiration estimates based on remote sensing approaches with a classical climate data driven method, *AUC Geographica*, 2020, vol. 55, no. 2, pp. 165–182. https://doi.org/10.14712/23361980.2020.12
145. Wagner, W., Hahn, S., Kidd, R., Melzer, T., Bartalis, Z., Hasenauer, S., Figa-Saldan, J., de Rosnay, P., Jann, A., Schneider, S., Komma, J., Kubu, G., Brugger, K., Aubrecht, C., Zuger, J., Gangkofner, U., Kienberger, S., Brocca, L., Wang, Y., Blöschl, G., Eitzinger, J., Steinnocher, K., Zeil, P., and Rubel, F., The ASCAT soil moisture product: a review of its specifications, validation results, and emerging applications, *Meteorol. Z.*, 2013, vol. 22, no. 1, pp. 5–33.
146. Wang, W., Huang, D., Wang, X.-G., Liu, Y.-R., and Zhou F., Estimation of soil moisture using trapezoidal relationship between remotely sensed land, surface temperature and vegetation index, *Hydrol. Earth Syst. Sci.*, 2011, vol. 15, pp. 1699–1712. www.hydrol-earth-syst-sci.net/15/1699/2011/. https://doi.org/10.5194/hess-15-1699-2011
147. Wang, Y., Zhang, S., and Chang, X., Evapotranspiration estimation based on remote sensing and the SEBAL model in the Bosten Lake Basin of China, *Sustainability*, 2020, vol. 12, pp. 7293. https://doi.org/10.3390/su12187293
148. Wie, W., Pang, S., Wang, X., Zhou, L., Xie, B., Zhou, J., and Li, C. Temperature vegetation precipitation dryness index (TVPDI)-based dryness–wetness monitoring in China, *Rem. Sens. Environ.*, 2020, vol. 248, 111957. https://doi.org/10.1016/j.rse.2020.111957
149. WIGOS https://public.wmo.int/en/about-us/vision-and-mission/wmo-integrated-global-observing-system.
150. WIGOS Highway https://ane4bf-datap1.s3.eu-west-1.amazonaws.com/wmod8_gcos/s3fs-public/2018_10_31_wigos-highway_uganda_0.pdf?ydrJDTLweQBhmZljgcUwuXLPT.
151. Wu, K., Ryu, D., Nie, L., and Shu, H., Time-variant error characterization of SMAP and ASCAT soil moisture using Triple Collocation Analysis, *Rem. Sens. Environ.*, vol. 256, 2021. 112324. https://doi.org/10.1016/j.rse.2021.112324
152. Wulfmeyer, V., Turner, D.D., Baker, B., Banta, R., Behrendt, A., Bonin, T., Brewer, W.A., Buban, M., Choukulkar, A., Dumas, E., Hardesty, R.M., Heus, T., Ingwersen, J., Lange, D., Lee, T.R., Metzendorf, S., Muppa, S.K., Meyers, T., Newsom, R., Osman, M., Raasch, S., Santanello, J., Senff, C., Späth, F., Wagner, T., Weckwerth, T., A new research approach for observing and characterizing land-atmosphere feedback, *Bull. Am. Met. Soc.*, 2018, no. 8, pp. 1639–1668.
153. Xia, T., Kustas, W.P., Anderson, M.C., Alfieri, J.G., Gao, F., McKee, L., Prueger, J.H., Geli, H.M.E., Neale, C.M.U., Sanchez, L., Alsina, M.M., Wang, Z., Mapping evapotranspiration with high-resolution aircraft imagery over vineyards using one- and two-source modeling schemes, *Hydrol. Earth Syst. Sci.*, 2016, vol. 20, pp. 1523–1545. https://doi.org/10.5194/hess-20-1523-2016
154. Xia, Y.L., Hao, Z.C., Shi, C.X., Li, Y.H., Meng, J., Xu, T.R., Wu, X.Y., and Zhang, B.Q., Regional and global land data assimilation systems: Innovations, challenges, and prospects, *J. Meteorol. Res.*, 2019, vol. 33, no. 2, pp. 1–31. https://doi.org/10.1007/s13351-019-8172-4
155. Xia, Y., Mitchell, K., Ek, M., Sheffield, J., Cosgrove, B., Wood, E., Luo, L., Alonge, C., Wei, H., Meng, J., Livneh, B., Lettenmaier, D., Koren, V., Duan, Q., Mo, K., Fan, Y., and Mocko, D., Continental-scale water and energy flux analysis and validation for the North American Land Data Assimilation System Project Phase 2 (NLDAS-2). 1. Intercomparison and application of model products, *J. Geophys. Res. Atm.*, 2012, vol. 3. D03109. https://doi.org/10.1029/2011JD016048
156. Yao, P.P., Shi, J.C., Zhao, T.J., Lu, H.L., Al-Yaari, A., Rebuilding long time series global soil moisture products using the neural network adopting the microwave vegetation index, *Remote Sens.*, 2017, vol. 9, no. 1, pp. 35–61. https://doi.org/10.3390/rs9010035
157. Ye, N., Walker, J.P., Wu, X., de Jeu, R., Gao, Y., Jackson, T.J., Jonard, F., Kim, E., Merlin, O., Pauwels, V.R.N., Renzullo, L.J., Rüdiger, C., Sabaghy, S., von Hebel, C., Yueh, S.H., and Zhu, L., The soil moisture active passive experiments: validation of the SMAP products in Australia, *IEEE Transactions GeoSci. Remote Sens.*, 2021, vol. 59, no. 4, pp. 2922–2939. https://doi.org/10.1109/TGRS.2020.3007371
158. Zeng, J., Li, Z., Chen, Q., Bi, H., Qiu, J., and Zou, P., Evaluation of remotely sensed and reanalysis soil moisture products over the Tibetan Plateau using in-situ observations, *Remote Sens. Environ.*, 2015, vol. 163, pp. 91–110. https://doi.org/10.1016/j.rse.2015.03.008
159. Zhang, K., Chao, L.-J., Wang, Q.-Q., Huang, Y.-C., Liu, R.-H., Hong, Y., Tu, Y., Qu, W., and Ye, J.-Y., Using multi-satellite microwave remote sensing observations for retrieval of daily surface soil moisture across China, *Water Sci. Engine*, 2019, vol. 12, no. 2, pp. 85–97. https://doi.org/10.1016/j.wse.2019.06.001

160. Zhang, K., Kimball, J.S., and Running, S.W., A review of remote sensing based actual evapotranspiration estimation, *WIREs Water*, 2016, vol. 3, no. 6, pp. 834–853.
https://doi.org/10.1002/wat2.1168

161. Zhang, Q., Fan, K., Singh, V.P., Sun, P., and Shi, P., Evaluation of remotely sensed and reanalysis soil moisture against in situ observations on the Himalayan-Tibetan Plateau, *J. Geophys. Res. Atm.*, 2018, vol. 123, pp. 7132–7148.
https://doi.org/10.1029/2017JD027763

162. Zhang, Y., He, B., Guo, L., Liu, J., and Xie, X., The relative contributions of precipitation, evapotranspiration, and runoff to terrestrial water storage changes across 168 river basins, *J. Hydrol.*, 2019, vol. 579. 124194.
https://doi.org/10.1016/j.jhydrol.2019.124194

163. Zhang, Y., Leuning, R., Chiew, F.H.S., Wang, E., Zhang, L., Liu, C., Sun, F., Peel, M.C., Shen, Y., and Jung, M., Decadal trends in evaporation from global energy and water balances, *J. Hydrometeorol.*, 2012, vol. 13, pp. 379–391.
https://doi.org/10.1175/JHM-D-11-012.1

164. Zhao, T., Hu, L., Shi, J., Lü, H., Li, S., Fan, D., Wang, P., Geng, D., Kang, C.S., and Zhang, Z., Soil moisture retrievals using L-band radiometry from variable angular ground-based and airborne observations, *Remote Sens. Environ.*, 2020, vol. 248. 111958.

165. Zhao, T., Shi, J., Entekhabi, D., Jackson, T.J., Hu, L., Peng, Z., Yao, P., Li, S., and Kang, C.S., Retrievals of soil moisture and vegetation optical depth using a multi-channel collaborative algorithm, *Remote Sens. Environ.*, 2021, vol. 257. 112321.
https://doi.org/10.1016/j.rse.2021.112321

166. Zhao, T., Shi, J., Lv, L., Xu, H., Chen, D., Cui, Q., Jackson, T.J., Yan, G., Jia, L., Chen, L., Zhao, K., Zheng, X., Zhao, L., Zheng, C., Ji, D., Xiong, C., Wang, T., Li, R., Pan, J., Wen, J., Yu, C., Zheng, Y., Jiang, L., Chai, L., Lu, H., Yao, P., Ma, J., Lv, H., Wu, J., Zhao, W., Yang, N., Guo, P., Li, Y., Hu, L., Geng, D., Zhang, Z., Soil moisture experiment in the Luan River supporting new satellite mission opportunities, *Remote Sens. Environ.*, 2020, vol. 240. 111680.
https://doi.org/10.1016/j.rse.2020.111680

167. Zhu, B., Song, X., Leng, P., Sun, C., Wang, R., and Jiang, X., A novel simplified algorithm for bare surface soil moisture retrieval using L-band radiometer, *ISPRS Int. J. Geo-Inf.*, 2016, vol. 5, no. 8, pp. 143.
https://doi.org/10.3390/ijgi5080143

APPENDIX

ABBREVIATIONS USED

WMO, World Meteorological Organization

KUREX, Kursk experiment (1988 and 1991)

LR MS, Low-Resolution Multichannel Scanner

ALOS, Advanced Land Observing Satellite

AMSR, Advanced Microwave Scanning Radiometer

AMSU-B, Advanced Microwave Sounding Unit-B

ASAR, Advanced Synthetic Aperture Radar

ASCAT, Advanced Scatterometer

ASTER, Advanced Spaceborne Thermal Emission and Reflection Radiometer

AVHRR, Advanced Very High-Resolution Radiometer

AW3D30, ALOS Global Digital Surface Model with a 30-m Resolution

BAHC, Biospheric Aspects of the Hydrological Cycle (core project of IGBP)

BARC, Beltsville Agricultural Research Center

BHOA, Balance Hidrolygico Operativo para el Agro

BOREAS, Boreal Ecosystem-Atmosphere Study

BPNN, Back Propagation Neural Network

CCI, Climate Change Initiative

CHELSA, Climatologies at High Resolution for the Earth's Land Surface Areas

CRU, Climate Research Union

CSIRO, Commonwealth Scientific and Industrial Research Organization

DAAC, Distributed Active Archive Center for Biogeochemical Dynamics

ECMWF, European Centre for Medium-Range Weather Forecasts

ECV, Essential Climate Variables

ERA-Interim TESSEL, ERA-Interim Tiled ECMWF's Scheme for Surface Exchanges over Land

EROS, Earth Resources Observation and Science center in Sioux Falls, South Dakota, USA

ERS, European Remote Sensing satellite

ESA, European Space Agency

ESA CCI, European Space Agency Climate Change Initiative

ESDAC, European Soil Data Centre

EUMETSAT, European Organization for the Exploitation of Meteorological Satellites

FAO, Food and Agriculture Organization of the United Nations

FAPAR, Fraction of Absorbed Photosynthetically Active Radiation

FIFE project, First ISLSCP Field Experiment (1987 and 1989)

GCOM-W1 and GCOM-C1, Global Change Observation Mission, Water and Climate

GCOS, Global Climate Observing System

GEOS-5 DAS, Goddard Earth Observing System-5 Data Assimilation System

GEWEX, Global Energy and Water Cycle EXchanges Project

GLASS, Global LAnd Surface Satellite

GLCC, Global Land Cover Characterization

GLDAS, Global Land Data Assimilation System

GLEAM, Global Land Evaporation: the Amsterdam Methodology

GMS, Geostationary Meteorological Satellite

GNSS, Global Navigation Satellite System

GOES, Geostationary Operational Environmental Satellite

GPCC, Global Precipitation Climatology Centre

GPCP, Global Precipitation Climatology Project

GRACE-FO, Gravity Recovery and Climate Experiment-Follow-On

GRDC, Global Runoff Data Centre

GSWP, Global Soil Wetness Project

Hyperion, Space-Based Imaging Spectrometer

H-SAF, Satellite Application Facility on Support to Operational Hydrology and Water Management

HWSD, Harmonized World Soil Database

ICESat-2, Ice, Cloud, and Land Elevation Satellite-2

IGBP, International Geosphere-Biosphere Programme

IRI/LDEO CDL, International Research Institute/Lamont-Doherty Earth Observatory Climate Data Library

ISBA model, Interactions between Soil–Biosphere–Atmosphere land surface model

ISD, Integrated Surface Database

ISLSCP II, International Satellite Land Surface Climatology Project, Initiative II, part of the GEWEX project

ISMN, International Soil Moisture Network

JAXA, Japan Aerospace Exploration Agency

LAFE, Land Atmosphere Feedback Experiment

LAI, Leaf Area Index

LAS, Large Aperture Scintillometer

LDAS, Land Data Assimilation System

LE, Latent Heat Flux

LISFLOOD, rainfall-runoff model

LPRM, Land Parameter Retrieval Model

LSA SAF, Land Surface Analysis Satellite Applications Facility

LSM, Land Surface Model

LST, Land Surface Temperature

LUCAS, Land Use/Cover Area frame statistical Survey

MERRA, Modern-Era Retrospective analysis for Research and Applications

Meteosat, Meteorological Satellite (geostationary satellite Meteosat Second Generation, MSG)

MetOp, Meteorological Operational satellite

METRIC, Mapping Evapotranspiration at High Resolution with Internalized Calibration

MIRAS, Microwave Imaging Radiometer with Aperture Synthesis

MODIS, MODerate resolution Imaging Spectroradiometer

MVI, Microwave Vegetation Index

NASA, National Aeronautics and Space Administration

NCEI, National Centres for Environmental Information

NDVI, Normalized Difference Vegetation Index

NLDAS, North American Land Data Assimilation System

NN, Neural Network

NOAA, National Oceanic and Atmospheric Administration

NGDC, National Geophysical Data Center

NPP, Net Primary Productivity

NRCS, Natural Resources Conservation Services

OLI, Operational Land Imager

ORNL, Oak Ridge National Laboratory in Oak Ridge, Tennessee, USA

OSCAR, Observing Systems Capability Analysis and Review

PAR, Photosynthetically Active Radiation

PLIS, Polarimetric L-band Imaging Scatterometer

PLMR, Polarimetric L-band Multibeam Radiometer

PML, Penman-Monteith-Leuning

PRISM, Panchromatic Remote-sensing Instrument for Stereo Mapping

PROBA, PRoject for On-Board Autonomy

RMSE, Root Mean Square Error

SCAN, Soil Climate Analysis Network

SEB, Surface Energy Balance

SEBAL, Surface Energy Balance Algorithm for Land

SEBS, Surface Energy Balance System

SEVIRI, Spinning Enhanced Visible Infra-Red Imager

SM, Soil Moisture

SMAP, Soil Moisture Active Passive

SMMR, Scanning Multichannel Microwave Radiometer

SMOS, Soil Moisture and Oceans Salinity

SNPP, Suomi National Polar-orbiting Partnership

SPI, Standardized Precipitation Index

SPOT, Satellite Pour l'Observation de la Terre

SRTM, Shuttle Radar Topography Mission

SSM/I, Special Sensor Microwave/Imager

SVAT, Soil Vegetation Atmosphere Transfer

SWE, Snow Water Equivalent

SWI, Soil Water Index

SWIR, shortwave infrared

SWOT, Surface Water and Ocean Topography

TIRS, Thermal Infrared Sensor

TRMM, Tropical Rainfall Measuring Mission

TRMM-TMI, TRMM Microwave Imager

TSEB, Two-Source Energy Balance

TVPDI, Temperature Vegetation Precipitation Dryness Index

TWRS, Terrestrial Water Resources Satellite

USDA, United States Department of Agriculture

USGS, United States Geological Survey

USGS LCI, USGS Land Cover Institute, USGS Land Cover Database

VCF product, Vegetation Continuous Fields product

VI, Vegetation Index

VIIRS, Visible Infrared Imaging Radiometer Suite

VNIR, visible and near-infrared

WCOM, Water Cycle Observation Mission

WCRP, World Climate Research Programme

WDI, Water Deficit Index

WHYCOS, World Hydrological Cycle Observing System

WIGOS, WMO Integrated Global Observing System

Windsat, Coriolis satellite with WindSat spaceborne polarimetric microwave radiometer on board